Available online at www.sciencedirect.com

ScienceDirect

Underground Space 25 (2025) 156–175

www.keaipublishing.com/undsp

Research Paper

Towards trustworthy excavation-induced risk warning for adjacent building: A Bayesian reasoning based probabilistic deep learning method

Yue Pan [a], Xuyang Li [a], Jianjun Qin [a,*], Jinjian Chen [a], Paolo Gardoni [b]

[a] State Key Laboratory of Ocean Engineering, Shanghai Key Laboratory for Digital Maintenance of Buildings and Infrastructure, School of Ocean and Civil Engineering, Shanghai Jiao Tong University, Shanghai 200240, China

[b] Department of Civil and Environmental Engineering, University of Illinois at Urbana–Champaign, Urbana IL 61801-2352 IL, USA

Received 11 August 2024; received in revised form 27 April 2025; accepted 31 May 2025
Available online 19 September 2025

Abstract

Foundation pit excavation for underground space development inevitably disrupts the surrounding soil, raising safety concerns for adjacent buildings. To address the need for an intelligent and trustworthy warning of the excavation-induced risk for adjacent buildings, this study develops a hybrid deep learning framework for probabilistic modeling (PM) with a long short-term memory (LSTM) neural network (termed as PM-LSTM). The proposed framework incorporates Bayesian reasoning and a bidirectional mechanism to enhance its predictive capabilities. The forward learning process enables the dynamic estimation of the probability that adjacent buildings will experience varying levels of risk over time, as new data is incorporated. Meanwhile, it can precisely calculate the first exceeding probability of the adjacent building entering an extremely high-risk level daily, facilitating early warning triggers. Besides, the reverse learning process leverages Bayesian reasoning to identify the most influential response parameters of the foundation pit, serving as key checkpoints for excavation monitoring. It further calculates the posterior probabilities and their intervals for each response parameter under the assumption of a specific risk state for adjacent structures. These insights enable the formulation of proactive risk mitigation measures. The proposed PM-LSTM framework is validated through a case study of the excavation project at Zone A of Jing'an Temple Station on Shanghai Metro Line 14. Comparative analyses further demonstrate the robustness of the framework, underscoring its potential as a reliable decision-making tool for risk analysis and management in complex and uncertain underground engineering projects.

Keywords: Deep excavation; Risk assessment; Long and short-term memory neural network; Probabilistic modeling; Bayesian reasoning

1 Introduction

Deep foundation excavation is commonly used for underground space development (Jin et al., 2021), but it can negatively affect surrounding soils and adjacent structures (Pan et al., 2025; Shen et al., 2023; Zhang et al., 2022; Zhou et al., 2024). Vertical displacement is a key indicator of excavation-induced risks to nearby buildings. Traditional prediction methods, such as empirical approaches, are more suited for early-stage projects but face challenges in delivering the precision and adaptability required during the later stages. Numerical simulations (You & Tian, 2023) offer an alternative but are hindered by the extensive time required for parameter calibration. Recently, artificial intelligence (AI) has emerged as a potential frontier in the construction industry (Pan & Zhang, 2023; Phoon et al., 2024). However, most current AI-based approaches focus on single-value predictions, overlooking geotechnical and model uncertainties, which undermines risk analysis reliability (Pan, Qin, Hou, & Chen, 2024; Pan, Qin, Zhang, Pan, & Chen, 2024). Meanwhile, these approaches often struggle to capture temporal

* Corresponding author.
E-mail address: jianjunqin@sjtu.edu.cn (J. Qin).
Peer review under the responsibility of Tongji University

https://doi.org/10.1016/j.undsp.2025.05.006
2467-9674/© 2025 Tongji University. Publishing Services by Elsevier B.V. on behalf of KeAi Communications Co. Ltd.
This is an open access article under the CC BY-NC-ND license (http://creativecommons.org/licenses/by-nc-nd/4.0/).

dependencies and manage complex and multidimensional inputs.

Regarding this, this study leverages deep learning techniques, specifically long short-term memory (LSTM) networks, for time series forecasting (Fu et al., 2024; Xue et al., 2022; Zhang et al., 2022). LSTM excels at capturing long-range dependencies in sequential data, providing high-precision, stable, and reliable spatiotemporal predictions. Despite their effectiveness, uncertainties in monitoring point configuration, environmental factors, and model limitations can lead to discrepancies between observed and predicted outcomes (Wang et al., 2025). To address this, probabilistic modeling (PM) can be integrated with LSTM to form the PM-LSTM model, thereby enhancing prediction robustness. This integration focuses on identifying the probability distributions and statistical features of monitoring data, minimizing prediction loss. As demonstrated by Qin (2018) and Pan and Qin (2022) in their dual-model estimation approach for uncertain wind speeds, this method can be applied to reconstruct excavation-related parameters, thereby improving the accuracy of temporal predictions for excavation-induced risks.

Existing studies primarily focus on risk prediction, yet the practical use of PM-LSTM's outputs for monitoring alerts and operational control remains underexplored. While the PM-LSTM model provides reliable excavation-induced risk predictions under uncertainty, determining risk levels for adjacent buildings typically relies on engineering specifications and on-site experience. A five-level risk warning system, based on building settlement values, is commonly used in excavation engineering (Zeng et al., 2023). Additionally, determining the probability of a building first entering a risk state can be addressed through the concept of first-exceeding risk probability, which quantifies the likelihood of reaching a specific risk level at a given time step. Rooted in Bayesian reasoning, this approach utilizes prior information and settlement prediction distributions to continuously update the model, refining the posterior distribution of building settlement over time.

The PM-LSTM model, integrated with the Bayesian reasoning process, offers valuable insights into a building's risk status and provides early warnings of excavation-induced risk. However, it lacks explicit guidance for stakeholders. To address this, a set of response parameters associated with the foundation pit—directly influenced by excavation conditions—is used to train the deep learning model (Lin et al., 2022). Therefore, statistically determining the range of these parameters across different risk states can inform data-driven safety management during deep excavation. Leveraging the diagnostic reasoning inherent in Bayesian processes, the PM-LSTM model can be implemented in reverse to identify the threshold intervals of foundation pit response parameters that may trigger building risks. Given the absence of studies addressing the bidirectional learning capability of the PM-LSTM in risk analysis, this work aims to fill this research gap.

In summary, this study aims to develop a reliable time-dependent Bayesian reasoning-based probabilistic deep learning prediction model named PM-LSTM with a bidirectional learning mechanism toward trustworthy excavation-induced risk warning for adjacent buildings. The study addresses three key questions: (1) How to develop a hybrid model integrating probabilistic modeling and deep learning to comprehensively learn from monitoring time-series data collected from an excavation project associated with uncertainties, aiming to capture the complicated interaction between the real-time risk of the excavation-induced building and the foundation pit response parameters? (2) How to extend the practical value of forward learning into assessing the probabilities of the adjacent building entering different risk states for the first time at each time step, ensuring timely risk warnings that prompt immediate attention? (3) How to estimate the response of excavation and guide the corresponding countermeasures to reduce or even to minimize the occurrence probability of risk events on the adjacent building?

The remaining structure of this paper is as follows. Section 2 introduces the proposed Bayesian reasoning-based PM-LSTM method. Section 3 validates the applicability of PM-LSTM in an excavation project of Shanghai Metro. Section 4 conducts comparative experiments to validate the effectiveness and robustness of PM-LSTM. Section 5 summarizes the key research findings.

2 Proposed framework

Figure 1 outlines the proposed approach for assessing excavation-induced risks to adjacent buildings in three steps. First, data is collected and preprocessed for training a hybrid deep learning model. Second, the PM-LSTM model, which combines probabilistic modeling with LSTM, is developed and trained to predict ground settlement accounting for uncertainties in engineering practice. The third step involves post-analysis to identify key factors influencing settlement risks through sensitivity analysis and reverse learning. By incorporating Bayesian methods, the PM-LSTM model integrates uncertainty and prior knowledge, enhancing prediction reliability and supporting informed decision-making.

2.1 Monitoring data pre-processing

Automated data acquisition devices at the excavation site enable real-time monitoring, capturing a wealth of data on project safety. However, external factors and sensor inconsistencies can result in invalid data, such as errors and noise, compromising data quality. To ensure reliable risk assessment, a key step before PM-LSTM implementation is transforming raw data into a standardized format. This involves data scaling to optimize deep learning performance and performing a Kendall coefficient-based correlation analysis to validate the selected features for model training. The procedure is detailed below.

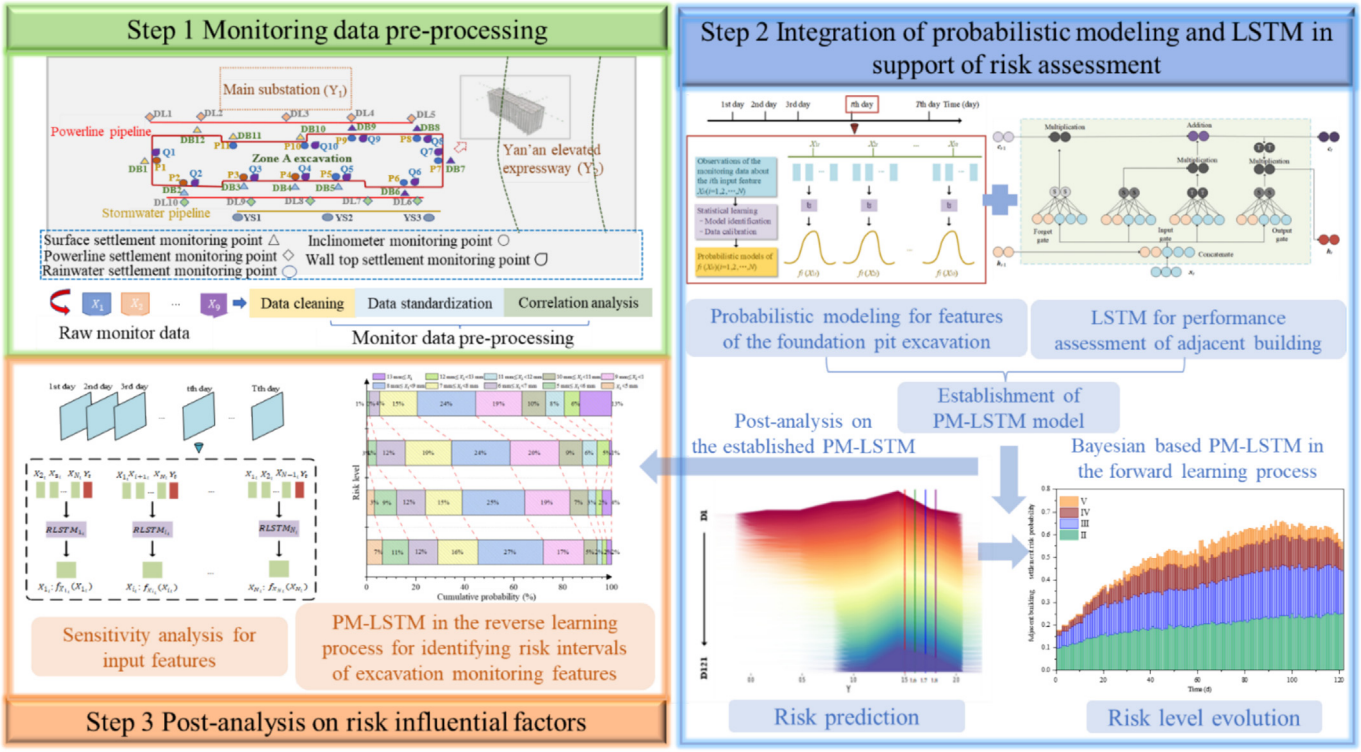

Fig. 1. Flowchart of the developed LSTM-based risk prediction approach.

Variations in the scales of data samples, stemming from inherent differences in target features and constraints imposed by measurement methodologies, present a prevalent challenge in modeling endeavors. Such differences in data scales can significantly impede the efficiency and performance of the intelligent model. To improve the model training efficiency and reduce operating costs, standard practice involves the implementation of data standardization as a precursor to model training. In this context, the utilization of the Min-Max scaler, as delineated in Eq. (1), serves to normalize data points into the range between 0 and 1 while preserving the integrity of the original data distribution.

$$x_{\text{scaled}} = \frac{x - x_{\min}}{x_{\max} - x_{\min}}, \tag{1}$$

where $x_{\min}$ and $x_{\max}$ represent the minimum and maximum values of the monitoring data, respectively.

To further understand the selected influential features in the risk prediction task, correlation analysis is implemented, serving as a mathematical tool for assessing the relationship between the risk object and influencing features. It is known that high correlation among features introduced into the deep learning model can significantly impact prediction accuracy and operational efficiency. Therefore, eliminating highly correlated input features before model training is a crucial aspect of data preprocessing (Song et al., 2023). Since the Kendall coefficient has unique advantages in dealing with time-series data and small-sample data, it is adopted here to measure time-series correlation effects between the excavation monitoring feature data. Let (X, Y) be a bivariate random variable with cumulative distribution function $H(x,y)$. The Kendall coefficient is defined in Eqs. (2) and (3). It aims to identify and remove highly correlated features. When features are too correlated with one another, they can negatively impact the model's prediction accuracy and operational efficiency.

$$\begin{aligned} R_{\text{k}}(H) &= E_H[\text{sign}((X_1 - X_2)(Y_1 - Y_2))] \\ &= 2P_H[(X_1 - X_2)(Y_1 - Y_2) > 0] - 1, \end{aligned} \tag{2}$$

where $R_{\text{k}}(H)$ represents the rank correlation coefficient, E_H denotes the expected value of the samples from distribution H, and P_H represents the probability of samples in distribution H. (X_1, Y_1) and (X_2, Y_2) are sample pairs of (X, Y) independently drawn from distribution $H(x, y)$, respectively.

$$r_{\text{k}} = \frac{2}{n(n-1)} \sum_{i<j} \text{sign}\left[(X_i - X_j)(Y_i - Y_j)\right], \tag{3}$$

where n represents the total number of observations in the dataset, and X_i and Y_i represent the ith observation in the sample dataset, respectively. The correlation coefficient r_{k} ranges from -1 to 1 and is a consistent estimator of the population $R_{\text{k}}(H)$. It measures the ordered association between X_i and Y_i. If the rankings of X_i and Y_i are consistent (i.e., both rankings are the same), then $r_{\text{k}} = 1$. If the discrepancies between the two rankings are completely

inconsistent (i.e., one ranking is completely opposite to the other), then $r_k = -1$. If X_i and Y_i are independent, then r_k is approximately zero.

It is assumed that there are totally M features of the foundation pit excavation to be automatically collected, and n_i observations are available for the ith feature X_{it} $(i = 1, 2, \cdots, M)$ at each time step t $(t = 1, 2, \cdots, T)$. Through the Kendall coefficient-based correlation analysis, the original set of M features will be reduced to N features with lower correlation for the creation of subsequent datasets. That is to say, a total of $\sum_{i=1}^{N} n_i$ observations are available at each time step t for the N features $(X_{1t}, X_{2t}, \cdots, X_{Nt})$ of the foundation pit excavation. Meanwhile, n_d observations are available for the risk indicator about the adjacent building Y_t (e.g., ground settlement) at each time step t $(t = 1, 2, \cdots, T)$. For the sake of clarity in this discussion, the vectors $\boldsymbol{\alpha}_t$ and $\boldsymbol{y}_t$ are used to represent the set of $\sum_{i=1}^{N} n_i$ observations for the N input features $(X_{1t}, X_{2t}, \cdots, X_{Nt})$ of the foundation pit excavation and the set of the n_d observations for the risk indicator concerning the adjacent building Y_t at time step t respectively.

2.2 Bayesian based PM-LSTM in support of risk assessment of adjacent buildings

2.2.1 Probabilistic modeling for features of foundation pit excavation

Monitoring data from the deep excavation project inevitably suffers from substantial uncertainty caused by the complex and changeable geological environments. This uncertainty affects observations of both the N features of the foundation pit excavation and the excavation-induced risk to adjacent buildings at each time step. To address these uncertainties, a statistical technique called probabilistic modeling is applied to the monitoring data. The primary objective of incorporating uncertainties in excavation engineering is to gain a better understanding of excavation-induced risk conditions and to enhance the reliability of subsequent risk prediction tasks in practice. The core principle behind probabilistic modeling involves identifying appropriate probability distribution types and their statistical characteristics, with the goal of fitting the monitoring data associated with excavation features at each time step by minimizing a loss function. For the sake of discussion, the following vectors $\boldsymbol{\alpha}_t, \boldsymbol{\beta}_t, \boldsymbol{\xi}_t, \boldsymbol{\varphi}_t$ are introduced to represent the relevant sets.

$\boldsymbol{\alpha}_t$ is the set of the observations of the N features of the foundation pit excavation at time step t.

$\boldsymbol{\beta}_t$ is the set of the observations of the excavation-induced risk on the adjacent building at time step t.

$\boldsymbol{\xi}_t$ is the collection of the sets $\boldsymbol{\alpha}_1, \boldsymbol{\alpha}_2, \cdots, \boldsymbol{\alpha}_t$ (sets of the observations of the N features of the foundation pit excavation before and at time step t).

$\boldsymbol{\varphi}_t$ is the collection of the sets $\boldsymbol{\beta}_1, \boldsymbol{\beta}_2, \cdots, \boldsymbol{\beta}_t$ (sets of the observations of the excavation-induced risk on the adjacent building before and at time step t).

Nonparametric probability distribution estimation relies on available data, but real-world projects often face limited monitoring data. Our approach addresses this by using statistical learning methods that work effectively with smaller datasets, identifying probability distributions of the features on a daily basis using the available data. This allows reliable estimates even when the data set is relatively small. Herein, monitoring data from the foundation pit construction project is accumulated to form the observation set $\boldsymbol{\alpha}_t$. In subsequence, a statistical learning process (Eq. (4)) provides a feasible solution for transforming the input data into the probabilistic model $f_t(X_{1t}, X_{2t}, \cdots, X_{Nt})$. For an intuitive understanding, Fig. 2 takes the monitoring data of N features at the tth time step as an example to illustrate

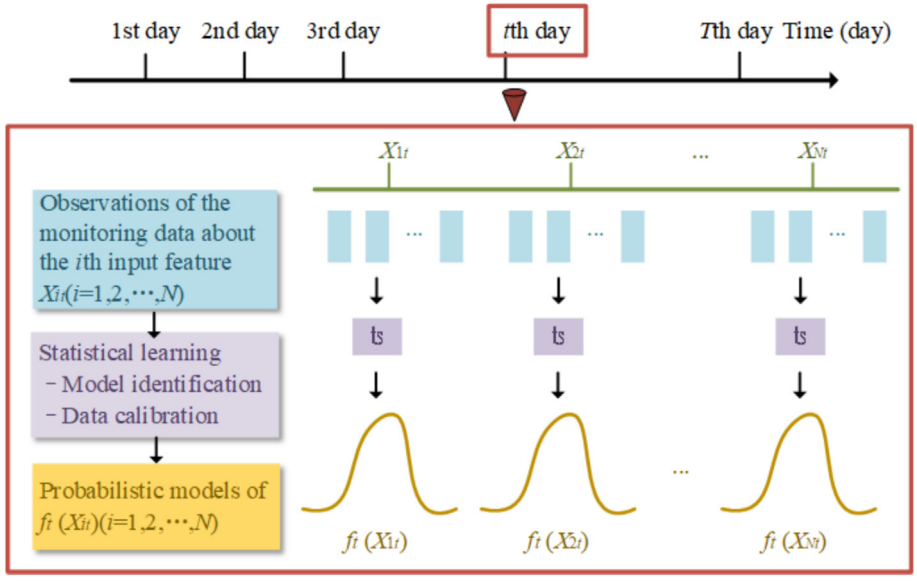

Fig. 2. Illustration of probabilistic modeling $f_t(X_{Nt})$ of foundation pit parameters under statistical learning at time step t.

the probabilistic modeling process of multiple daily data samples for excavation monitoring features. Statistical learning fits and calibrates data collected over time, identifying the appropriate probability distribution and calibrating its parameters via maximum likelihood estimation. This approach models uncertainties in the data, improving the reliability and robustness of the risk prediction model for the excavation project.

$$\boldsymbol{\alpha}_t \rightarrow f_t(X_{1t}, X_{2t}, \cdots, X_{Nt}). \tag{4}$$

Several probability distributions are well-established in engineering practice and can serve as candidates for modeling, including the normal distribution, log-normal distribution, and Weibull distribution. To be more specific, the normal distribution (also known as the Gaussian distribution) is one of the most common distributions in probability statistics. Its probability density function (PDF) is determined by two parameters: the mean μ and the variance σ^2. The normal distribution is symmetrical, with a bell-shaped curve. The log-normal distribution is particularly suited for modeling phenomena where data values range between 0 and positive infinity, such as settlement data that typically evolves from an initial value in one direction. The Weibull distribution is an important tool for reliability description and lifetime analysis. Unlike normal and log-normal distributions, the Weibull distribution has a probability density function that is monotonically decreasing or increasing. It is formed by two parameters: the scale parameter λ and the shape parameter k. After statistical learning, the optimal probability distribution for the monitoring feature data at each time step t can be determined using the evaluation metric called mean squared error (MSE) in Eq. (5), and parameters of the probabilistic model can also be determined accordingly. Such a probabilistic modeling process, as depicted in Fig. 2, can be iteratively applied to the monitoring data of N features across T time steps during excavation.

$$\mathrm{MSE} = \frac{1}{n}\sum_{1}^{n}\left(\bar{y}_i - y_i\right)^2, \tag{5}$$

where n is the data quantity, y_i represents the original value, and $\bar{y}_i$ denotes the predicted value from the candidate probability distribution.

2.2.2 Long short-term memory neural network (LSTM) for performance assessment of adjacent building

It is known that the standard LSTM consisting of the forget gate, the input gate, and the output gate has been extensively utilized in the time-series forecasting problem (Hochreiter & Schmidhuber, 1997). The cell structure of LSTM is provided in Fig. 3. To be more specific, the forget gate in Eq. (6) controls the received information from the previous memory cell. The input gate in Eq. (7) determines the new information to be added to update the memory cell. Therefore, the state of the memory cell can be updated according to Eq. (8). The output gate in Eq. (9) decides whether the existing information in the memory cell contributes to the output. As a result, the output in the current moment cell unit can be expressed as Eq. (10).

$$\boldsymbol{f}_t = \sigma(\boldsymbol{W}_{\mathrm{f}} \cdot [\boldsymbol{h}_{t-1}, \boldsymbol{x}_t] + \boldsymbol{b}_{\mathrm{f}}), \tag{6}$$

$$\boldsymbol{i}_t = \sigma(\boldsymbol{W}_{\mathrm{i}} \cdot [\boldsymbol{h}_{t-1}, \boldsymbol{x}_t] + \boldsymbol{b}_{\mathrm{i}}), \tag{7}$$

$$\boldsymbol{c}_t = \boldsymbol{f}_t \otimes \boldsymbol{c}_{t-1} + i_t \otimes (\tanh(\boldsymbol{W}_{\mathrm{c}} \cdot [\boldsymbol{h}_{t-1}, \boldsymbol{x}_t] + \boldsymbol{b}_{\mathrm{c}})), \tag{8}$$

$$\boldsymbol{o}_t = \sigma(\boldsymbol{W}_{\mathrm{o}} \cdot [\boldsymbol{h}_{t-1}, \boldsymbol{x}_t] + \boldsymbol{b}_{\mathrm{o}}), \tag{9}$$

$$\boldsymbol{h}_t = \boldsymbol{o}_t \cdot \tanh(\boldsymbol{c}_t), \tag{10}$$

where $\boldsymbol{h}_{t-1}$ is the hidden state from the previous cell, $\boldsymbol{x}_t$ is the input at the current moment, $\boldsymbol{c}_t$ is the output state of the current cell, $\boldsymbol{W}$ and $\boldsymbol{b}$ are the weight and bias, respectively (the subscript can either be the input gate i, output gate o, the forget gate f, or the memory cell c, depending on the activation being calculated), and symbol '⊗' represents the multiplication of all the elements in corresponding vectors.

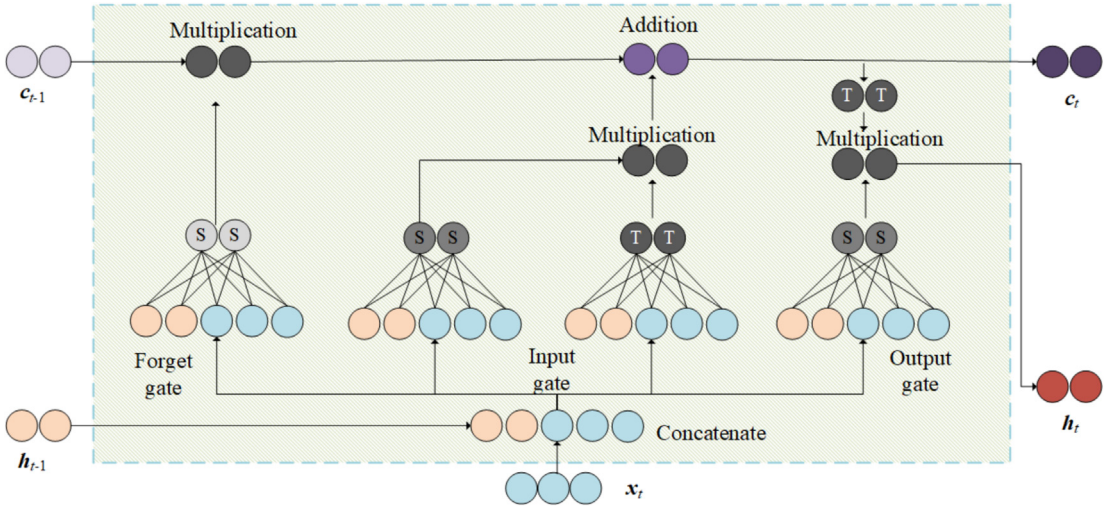

Fig. 3. Neural network architecture for a single LSTM cell.

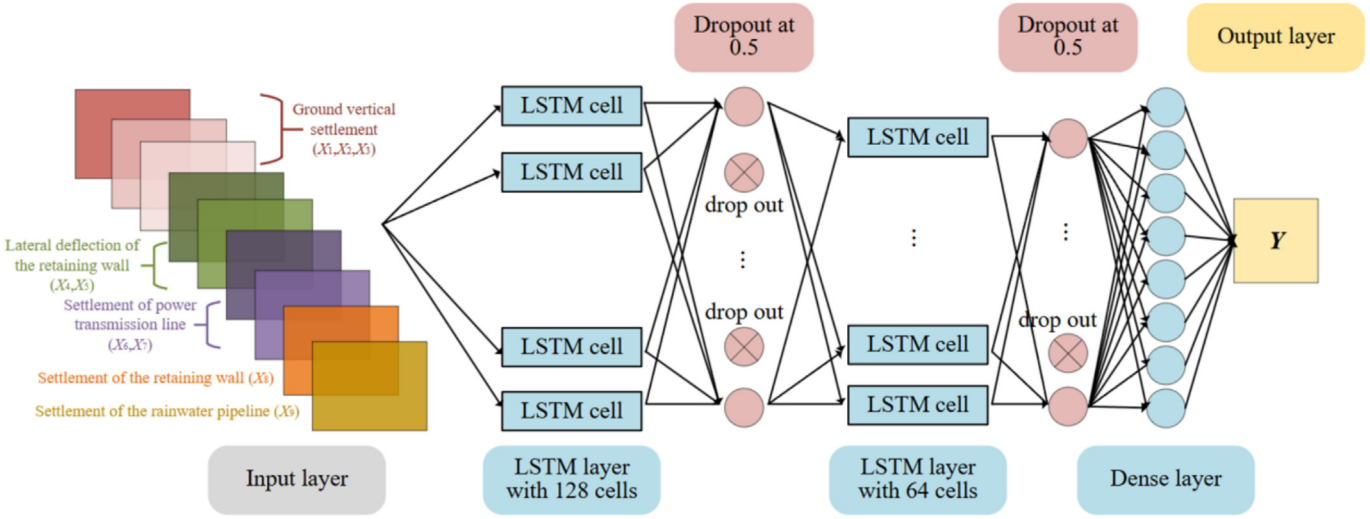

Fig. 4. Graphical illustration of the LSTM neural network structure.

The proposed PM-LSTM is built on a two-layer LSTM architecture, as shown in Fig. 4. To be more specific, the preprocessed monitoring data from foundation pit construction is fed into the LSTM for training, with feature selection being data-driven and context-specific. This enables the model to automatically capture relevant features and long-term temporal dependencies. The first and second LSTM blocks contain 128 and 64 cells, respectively, with dropout layers (0.5) after each block to prevent overfitting. A fully connected layer with ReLU activation enhances non-linearity expression, followed by a single neuron output layer to predict building risk. The MSE expressed in Eq. (5) is used as both the loss function and evaluation metric, with Adam as the optimizer. A smaller MSE indicates higher prediction accuracy. LSTM's memory mechanism allows it to capture temporal dependencies, making it ideal for time-series tasks, learning and evolving with more data.

2.2.3 Bayesian based PM-LSTM in the forward learning process in support of risk assessment

Given the feasibility of probabilistic modeling and the reliability of LSTM prediction, integrating these approaches offers a meaningful advancement in estimating adjacent building settlement values and their associated uncertainties, thereby enhancing risk status prediction and warning. At the initial time step ($t = 1$), the relationship between the excavation monitoring features $\boldsymbol{X}_{i1}(i = 1, 2, \cdots, N)$ and the excavation-induced settlement on the adjacent building $\boldsymbol{Y}_1$ in the form of a probability distribution is captured by the forward learning process of the PM-LSTM model Λ_1, as formulated in Eq. (11).

$$\Lambda_1 : f_1(\boldsymbol{X}_{i1}, \boldsymbol{X}_{i2}, \cdots, \boldsymbol{X}_{iN}) \xrightarrow{\Lambda_1} g_1(\boldsymbol{Y}_1). \tag{11}$$

At the second time step ($t = 2$), based on the observed excavation monitoring feature values $\boldsymbol{X}_{i2}(i = 1, 2, \cdots, N)$, the probabilistic model of the adjacent building settlement value $\boldsymbol{Y}_2$ is updated to $\widetilde{g}_2(\boldsymbol{Y}_2)$ following a Bayesian approach given in Eq. (12).

$$\widetilde{g}_2(\boldsymbol{Y}_2) \sim g_2(\boldsymbol{Y}_2|\boldsymbol{\xi}_2, \boldsymbol{\varphi}_1, \Lambda_1), \tag{12}$$

where $\widetilde{g}_2(\boldsymbol{Y}_2)$ is the updated probabilistic model given the set $\boldsymbol{\xi}_2, \boldsymbol{\varphi}_1, \Lambda_1$. Typically, the updated probabilistic model cannot be directly obtained through theoretical solutions, and herein numerical simulation is adopted to be an appropriate approach. Correspondingly, the PM-LSTM model Λ_2 can be expressed below.

$$\Lambda_2 : \left\{ \begin{matrix} f_1(\boldsymbol{X}_{1_1}, \boldsymbol{X}_{2_1}, \cdots, \boldsymbol{X}_{N_1}) \\ f_2(\boldsymbol{X}_{1_2}, \boldsymbol{X}_{2_2}, \cdots, \boldsymbol{X}_{N_2}) \end{matrix} \xrightarrow{\Lambda_2} \begin{matrix} g_1(\boldsymbol{Y}_1) \\ \widetilde{g}_2(\boldsymbol{Y}_2) \end{matrix} \right\}. \tag{13}$$

As the modeling process continues ($t > 2$), the probabilistic model of the adjacent building settlement value $\boldsymbol{Y}_t$ based on the observed excavation monitoring features on the construction site $\boldsymbol{X}_{it}(i = 1, 2, \cdots, N)$ is updated to $\widetilde{g}_t(Y_t)$ using a Bayesian approach in Eq. (14):

$$\widetilde{g}_t(\boldsymbol{Y}_t) \sim g_t(\boldsymbol{Y}_t|\boldsymbol{\xi}_t, \boldsymbol{\varphi}_{t-1}, \Lambda_{t-1}), \tag{14}$$

where $\widetilde{g}_t(\boldsymbol{Y}_t)$ represents the updated probabilistic model given the set $\boldsymbol{\xi}_t, \boldsymbol{\varphi}_{t-1}, \Lambda_{t-1}$, and the probabilistic model formulated based on the Bayesian method is shown in Eq. (15). The corresponding LSTM Λ_t is:

$$\Lambda_t : \left\{ \begin{matrix} f_1(\boldsymbol{X}_{1_1}, \boldsymbol{X}_{2_1}, \cdots, \boldsymbol{X}_{N_1}) \\ f_2(\boldsymbol{X}_{1_2}, \boldsymbol{X}_{2_2}, \cdots, \boldsymbol{X}_{N_2}) \\ \cdots \\ f_t(\boldsymbol{X}_{1_t}, \boldsymbol{X}_{2_t}, \cdots, \boldsymbol{X}_{N_t}) \end{matrix} \xrightarrow{\Lambda_t} \begin{matrix} g_1(\boldsymbol{Y}_1) \\ \widetilde{g}_2(\boldsymbol{Y}_2) \\ \cdots \\ \widetilde{g}_t(\boldsymbol{Y}_t) \end{matrix} \right\}. \tag{15}$$

The forward learning process is completed at the final time step T, and the probabilistic model sequence of adjacent building settlement values throughout the entire excavation process can be obtained: $g_1(\boldsymbol{Y}_1), \widetilde{g}_2(\boldsymbol{Y}_2), \cdots, \widetilde{g}_t(\boldsymbol{Y}_t)$. To sum up, the PM-LSTM implementation has been introduced in the following algorithm.

Algorithm Bayesian based PM-LSTM in the forward learning process.

Initialize with predefinition of mini batch size M, total time step T.
Formulate probabilistic models of daily monitoring feature data samples from the excavation pit $f_t(\boldsymbol{X}_{i_t})(i \in [1,N], t \in [1,T])$ through the statistical learning process ts.
Formulate the probabilistic model of the performance indicator of adjacent building $g_1(\boldsymbol{Y}_1)(t=1)$.
Specify the initial time step of monitoring j_0
for episode = 1, M do
  for j= 1, T do
    Generate samples of monitoring data β_j from the probabilistic model $\widetilde{g}_j(\boldsymbol{Y}_j)$
    Update the probabilistic model $\widetilde{g}_j(\boldsymbol{Y}_j)$ from the monitoring data α_j using a Bayesian approach: $\widetilde{g}_j(\boldsymbol{Y}_j) \sim g_j(\boldsymbol{Y}_j|\xi_j\varphi_{j-1}\Lambda_{j-1})$
    Update the probabilistic models of the performance indicator of adjacent building $\widetilde{g}_j(\boldsymbol{Y}_j)$ with the PM-LSTM Λ_{j-1} in a forward learning process:

$$\widetilde{g}_j(\boldsymbol{Y}_j) \sim g_j\left(\boldsymbol{Y}_j|\boldsymbol{\xi}_j, \boldsymbol{\varphi}_{j-1}, \Lambda_{j-1}\right)$$

$$\Lambda_j: \left\{\begin{array}{l} f_1(\boldsymbol{X}_{1_1}, \boldsymbol{X}_{2_1}, \cdots, \boldsymbol{X}_{N_1}) \\ f_2(\boldsymbol{X}_{1_2}, \boldsymbol{X}_{2_2}, \cdots, \boldsymbol{X}_{N_2}) \\ \cdots \\ f_t(\boldsymbol{X}_{1_t}, \boldsymbol{X}_{2_t}, \cdots, \boldsymbol{X}_{N_t}) \end{array}\right\} \xrightarrow{\Lambda_t} \left\{\begin{array}{c} g_1(\boldsymbol{Y}_1) \\ \widetilde{g}_2(\boldsymbol{Y}_2) \\ \cdots \\ \widetilde{g}_t(\boldsymbol{Y}_t) \end{array}\right\}$$

  end for
end for

Additionally, to enhance the applicability of PM-LSTM-based predictions for risk assessment, particular focus is given to quantifying the risk probability for adjacent buildings. A higher value of the excavation-induced risk on the adjacent building, represented by its ground settlement, means a higher-risk excavation condition. To quantify these risks, thresholds for the excavation-induced risk of the adjacent building $\varepsilon_1, \varepsilon_2, \varepsilon_3, \varepsilon_4 (\varepsilon_1 < \varepsilon_2 < \varepsilon_3 < \varepsilon_4)$ are set as the lower boundaries of the five different risk levels, donated by I, II, III, IV, V, respectively. Correspondingly, the probability of an adjacent building being at a specific risk level $P_{\mathrm{II}_t}, P_{\mathrm{III}_t}, P_{\mathrm{IV}_t}, P_{\mathrm{V}_t}$ at each time step t (t = 1, 2,$\cdots$, T) can be calculated using Eqs. (16)–(20), respectively. These probabilities represent the likelihood that the respective threshold is surpassed without exceeding the thresholds for higher risk levels at that time step.

$$P_{\mathrm{I}_t} = \Pr(\boldsymbol{Y}_t \le \varepsilon_1) = \begin{cases} \int_{-\infty}^{\varepsilon_1} g_1(y_1)\mathrm{d}y_1 & t=1 \\ \int_{-\infty}^{\varepsilon_1} \widetilde{g}_t(y_t)\mathrm{d}y_t & t=2,3,\cdots,T \end{cases} \tag{16}$$

$$P_{\mathrm{II}_t} = \Pr(\varepsilon_1 < \boldsymbol{Y}_t \le \varepsilon_2) = \begin{cases} \int_{\varepsilon_1}^{\varepsilon_2} g_1(y_1)\mathrm{d}y_1 & t=1 \\ \int_{\varepsilon_1}^{\varepsilon_2} \widetilde{g}_t(y_t)\mathrm{d}y_t & t=2,3,\cdots,T \end{cases} \tag{17}$$

$$P_{\mathrm{III}_t} = \Pr(\varepsilon_2 < \boldsymbol{Y}_t \le \varepsilon_3) = \begin{cases} \int_{\varepsilon_2}^{\varepsilon_3} g_1(y_1)\mathrm{d}y_1 & t=1 \\ \int_{\varepsilon_2}^{\varepsilon_3} \widetilde{g}_t(y_t)\mathrm{d}y_t & t=2,3,\cdots,T \end{cases} \tag{18}$$

$$P_{\mathrm{IV}_t} = \Pr(\varepsilon_3 < \boldsymbol{Y}_t \le \varepsilon_4) = \begin{cases} \int_{\varepsilon_3}^{\varepsilon_4} g_1(y_1)\mathrm{d}y_1 & t=1 \\ \int_{\varepsilon_3}^{\varepsilon_4} \widetilde{g}_t(y_t)\mathrm{d}y_t & t=2,3,\cdots,T \end{cases} \tag{19}$$

$$P_{\mathrm{V}_t} = \Pr(\boldsymbol{Y}_t \ge \varepsilon_4) = \begin{cases} \int_{\varepsilon_4}^{\infty} g_1(y_1)\mathrm{d}y_1 & t=1 \\ \int_{\varepsilon_4}^{\infty} \widetilde{g}_t(y_t)\mathrm{d}y_t & t=2,3,\cdots,T \end{cases} \tag{20}$$

where $y_t (t = 1,2,\cdots,T)$ is the realization of $\boldsymbol{Y}_t$.

In engineering practice, the first time step to exceed the corresponding settlement control value is crucial for efficient decision-making to protect adjacent buildings. Therefore, it is necessary to raise a critical concept named the first exceeding risk probability of excavation-induced settlement. This concept pertains to the likelihood of the settlement value of adjacent buildings surpassing the prescribed control threshold for the first time. It is noteworthy that the calculation of the first exceeding risk probability of excavation-induced settlement requires no occurrence of exceeding the settlement control value before the current time step t. Regarding this, Eq. (21) is carefully designed to assess the probability of adjacent buildings exceeding the maximum settlement control value for the first time at each time step t (t = 1,2,$\cdots$,T). Setting the maximum settlement control value too low is not advisable, as an excessively small value not only lacks significance for assessing excavation-induced settlement risks to adjacent buildings but also disrupts effective risk management practices. The threshold values for maximum settlement control in our manuscript are indeed suggested by on-site engineers based on their professional judgment, practical experience, and site-specific conditions.

$$P_{1\mathrm{V}_t} = \begin{cases} P_{1\mathrm{V}_t} & t=1 \\ \Pr(\boldsymbol{Y}_t \ge \varepsilon_4 \cap_{i=2,3,\cdots,t} \boldsymbol{Y}_i < \varepsilon_4) & t=2,3,\cdots,T \end{cases} \tag{21}$$

2.3 Bayesian based PM-LSTM in support of risk warning for adjacent buildings

2.3.1 Sensitivity analysis for input features regarding excavation-induced risk on adjacent buildings

As a popular post-analysis technique, sensitivity analysis can be directly applied to the established PM-LSTM model, aiming to discern the input features exerting a significant influence on the model's output. For one thing, sensitivity analysis aids in interpreting the PM-LSTM

model with the complex input–output mapping through quantitatively ranking the importance of excavation monitoring features in shaping predictions regarding excavation-induced risk on the adjacent building. For another, features identified as highly sensitive can be regarded as potential contributors to heightened risk probabilities concerning the adjacent building. This facilitates project managers in refining their focus, enabling them to make informed decisions to ensure safety and security.

To comprehensively examine the impact of variations across the entire input data space of excavation monitoring features on the PM-LSTM model output of the excavation-induced risk, sensitivity analysis typically employs Eq. (22) for computation. Hence, the interpretation of the risk influential factors influencing excavation-induced risk prediction primarily assumes a qualitative nature. A higher value of the sensitivity index derived from Eq. (22) signifies a greater influence of the respective feature on the targeted risk.

$$S_i = \frac{\partial \boldsymbol{Y}}{\partial \boldsymbol{X}_i} \cdot \frac{E[\boldsymbol{X}_i]}{E[\boldsymbol{Y}]}, \tag{22}$$

where S_i denotes the sensitivity of the parameter $\boldsymbol{X}_i (i = 1, 2, \cdots, N)$ to $\boldsymbol{Y}$.

2.3.2 Bayesian-based PM-LSTM in the reverse learning process in support of risk warning for adjacent buildings

The PM-LSTM in the reverse learning process can pave a new way to infer input features based on observations related to the building risk. The goal of developing an inverse version of PM-LSTM is to theoretically identify the risk intervals of excavation monitoring features, thereby determining a specific failure probability for the adjacent building while comprehensively considering uncertainties. Risk warning can be realized for the adjacent building if the risk intervals of excavation monitoring features are reached in engineering practice. This approach aids in formulating rational risk mitigation measures for the adjacent building.

Based on the obtained probabilistic model sequence of settlement values $g_1(\boldsymbol{Y}_1), \widetilde{g}_2(\boldsymbol{Y}_2), \cdots, \widetilde{g}_t(\boldsymbol{Y}_t)$, the established PM-LSTM needed to be implemented in an inverse direction to realize the identification of the risk intervals of excavation monitoring features. Analogous to the forward learning formulated in Eq. (11), the PM-LSTM model under reverse learning denoted as $R\Lambda_{1i}$ can build a non-linear relationship between adjacent building settlement values Y_t and excavation monitoring features $\boldsymbol{X}_{it} (i = 1, 2, \cdots, N)$ at the time step $(t = 1)$ by Eq. (23). Thereafter, at time step $t \geq 2$, the corresponding PM-LSTM under reverse learning denoted as $R\Lambda_{ti}$ can be generally defined by Eq. (24).

$$R\Lambda_{1i}: g_1(\boldsymbol{Y}_1) \overset{R\Lambda_{1i}}{\rightarrow} \boldsymbol{h}_t(\boldsymbol{X}_{i1}) (i = 1, 2, \cdots, N), \tag{23}$$

$$R\Lambda_{ti}: \begin{Bmatrix} g_1(\boldsymbol{Y}_1) & \boldsymbol{h}_1(\boldsymbol{X}_{i1}) \\ \widetilde{g}_2(\boldsymbol{Y}_2) & \overset{R\Lambda_{ti}}{\rightarrow} \boldsymbol{h}_2(\boldsymbol{X}_{i2}) \\ \cdots & \cdots \\ \widetilde{g}_t(\boldsymbol{Y}_t) & \boldsymbol{h}_t(\boldsymbol{X}_{it}) \end{Bmatrix} (i = 1, 2, \cdots, N). \tag{24}$$

When the adjacent building reaches a certain risk level, the probability of excavation monitoring features at a certain interval can be obtained by Eq. (24). This updated probabilistic model facilitates the assessment of feature probabilities across various intervals. For example, given the condition that the adjacent building lies within the range $\varepsilon_x \leq \boldsymbol{Y}_t \leq \varepsilon_y$, Eq. (25) allows for the probability calculation of the ith feature falling within any designated range (e.g., $r_1 \leq \boldsymbol{X}_{it} \leq r_r$). This approach enables the rational identification of input configurations that lead to desired risk outcomes, thereby supporting effective risk warning and response strategies. That is to say, the key feature intervals with higher probabilities derived from Eq. (25) can be interpreted as risk intervals for triggering an early warning. Meanwhile, appropriate safety measures can be implemented to regulate these influential factors within specified intervals, mitigating risks proactively. Furthermore, as the excavation progresses, posterior information from previous time steps can serve as prior knowledge for updating future models. Thus, the PM-LSTM model, incorporating reverse learning, can be continually refined, empowering decision-makers to adjust risk management strategies and anticipate potential risk events.

$$\Pr\left(r_1 \leq \boldsymbol{X}_{it} \leq r_r | \varepsilon_x \leq \boldsymbol{Y}_t \leq \varepsilon_y\right) = \int_{r_1}^{r_r} \boldsymbol{h}_t\left(x_{it} | \varepsilon_x \leq \boldsymbol{Y}_t \leq \varepsilon_y\right). \tag{25}$$

3 Case study

3.1 Background

The PM-LSTM model with a bidirectional learning mechanism is validated through a case study of the excavation at Zone A of Jing'an Temple Station on Shanghai Metro. The excavation area spans 112.5 m in length, with a width of 29.7 m and a depth of 23.8 m. Positioned at the intersection of Yan'an Middle Road and Huashan Road, this target area is situated within densely urbanized surroundings characterized by existing pipes and buildings. Notably, the main substation, located less than 10 m from the deep excavation area, is particularly susceptible to long-term risks associated with the foundation pit construction project. Consequently, the necessity arises for long-term monitoring of excavation-induced risks, the establishment of systematic risk assessment criteria, and the implementation of protective measures. Monitoring equipment devices are strategically placed on the construction site to continuously monitor excavation responses. The corresponding monitoring points for different features

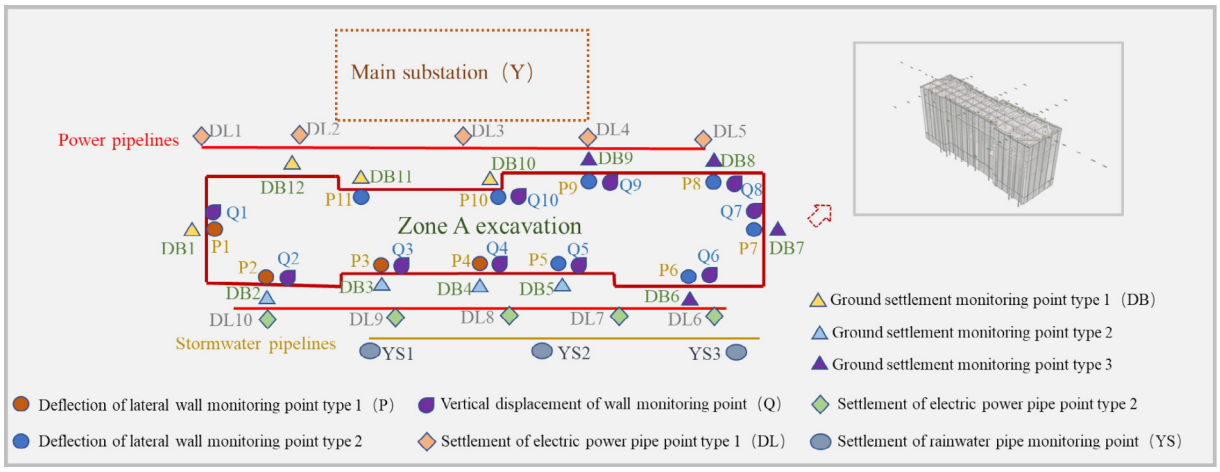

Fig. 5. Layout of the monitoring points in the foundation pit project area.

are delineated in Fig. 5. The arrangement of these monitoring points follows the national technical standard GB 50497—2019 (Ministry of Housing and Urban-Rural Development of the People's Republic of China, 2019).

3.2 Dataset preparation

To enhance prediction reliability and efficiency, it is necessary to extract several key features for dataset preparation. Herein, nine critical features, identified through engineering practice, are incorporated into the excavation-induced risk prediction model. These include ground settlement at the pit (X_1, X_2, X_3), lateral wall deflection (X_4, X_5), vertical wall displacement (X_6), settlement of the electric power pipe (X_7, X_8), and settlement of the rainwater pipe (X_9). To be more specific, features X_1–X_6 belong to the construction monitoring items, aiming to monitor the response of the targeted excavation system at different construction stages. Features X_7–X_9 relate to surrounding environment items, and their large value tends to cause cracks on the ground surface. As a case study, the monitoring data within 122 days (from 2018-08-18 to 2018-12-17) are taken out for deep investigation. This example helps clarify how these nine features were chosen based on engineering practice and the specific requirements of the case study.

To gain an intuitive understanding of the prepared dataset, these selected features are visualized in the excavation system of Fig. 6, and their statistical description is provided in Table 1. The measured data of each feature at each monitoring point are recorded in the format of a time series, as shown in Fig. 7. All of these temporal sequences are in the length of 122 days, resulting in a dataset of dimensions 122 × 46 (9 features across 46 monitoring points) from the monitoring system for deep learning model establishment.

Besides, the Kendall coefficient from Eqs. (2) and (3) is calculated to further validate the rationality of the selected features for the task of excavation-induced risk prediction. The correlation matrix is given in Fig. 8, where all Kendall's coefficients do not exceed 0.7, and most coefficients between the response features are below 0.6. This indicates the absence of highly correlated data, thereby avoiding potential overfitting issues in the predictive models.

3.3 PM-LSTM implementation

Following Section 2.2.1, the probabilistic modeling approach is employed to fit and model the limited monitoring data for the nine determined input features on a daily basis. Herein, three common types of probability distributions are utilized for data fitting, including the normal distribution, log-normal distribution, and Weibull distribution. Each distribution yields different effects on various data samples. To quantitatively evaluate the performance of different distributions, the MSE value is calculated, with the distribution exhibiting the lowest MSE value deemed the best fit for the data samples at that time step.

Take probabilistic modeling for the measured data on the first day as an example. Table 2 evaluates the performance of the three candidate distributions in fitting the first day of measured data of the nine identified features. For a more intuitive understanding, the corresponding probabilistic modeling results for the specific feature X_1 are provided in Fig. 9, where the MSE values for the three distributions are 0.23, 0.45, and 1.18, respectively. The smallest MSE value of 0.23 indicates that the normal distribution is suitable for fitting the data points of the feature X_1 on the first day (D_1–X_1). Similarly, the best-fit distribution for all measured data of nine features (X_1–X_9) on the first day can be easily determined based on the lowest MSE, which has been given in Fig. 10.

Following probabilistic modeling with the optimal distribution, Monte Carlo simulations are conducted to flexibly generate a sufficient number of multivariate samples jointly. This approach effectively addresses the issue of limited measured data while incorporating the inherent mea-

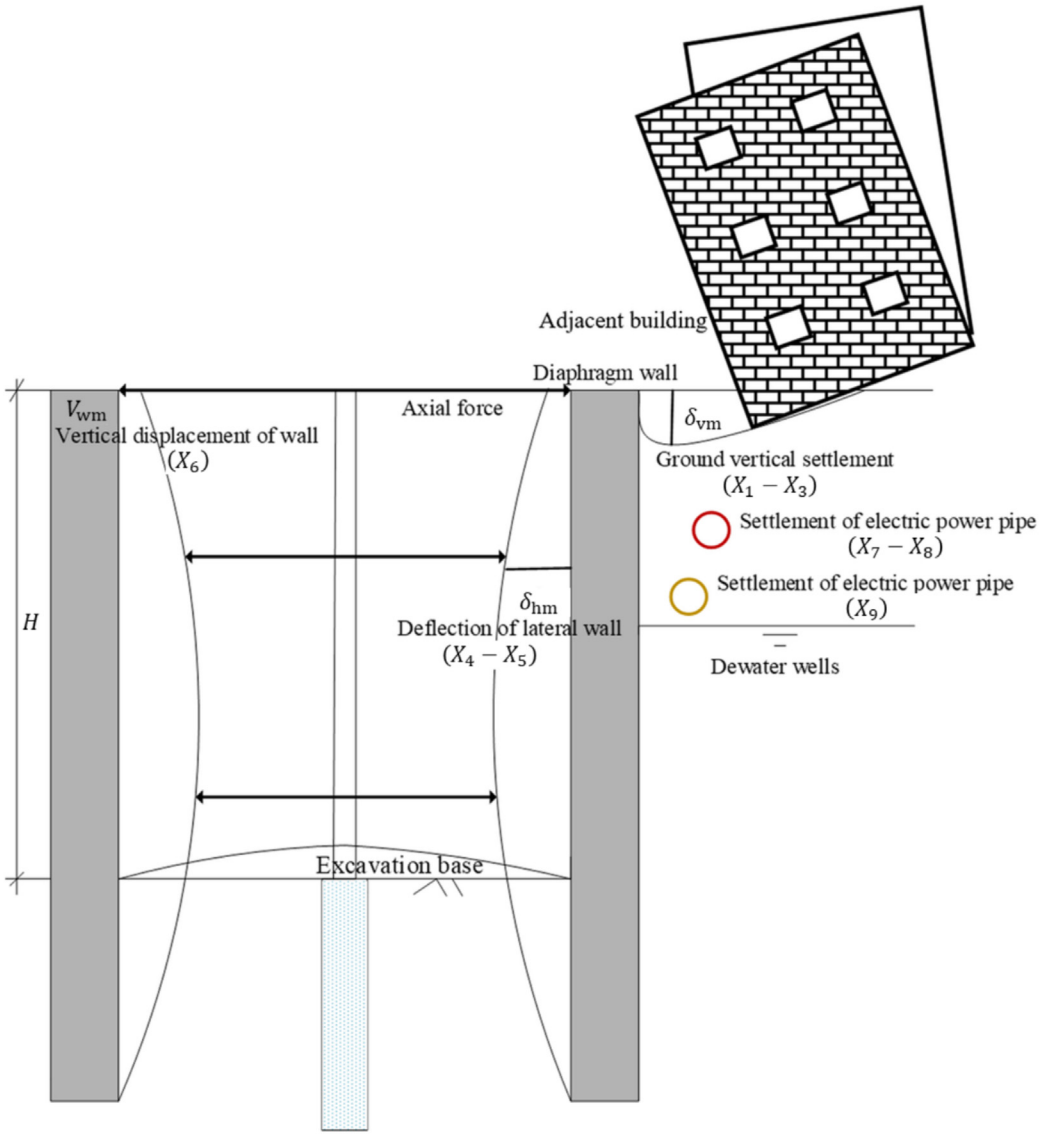

Fig. 6. Typical response in the foundation pit excavation system.

Table 1
Statistical description of the input features.

Feature	Description	Unit	Monitoring points	Mean	Std	Range
X_1	Ground vertical settlement-1	mm	DB2–DB5	7.25	3.22	[2.34, 15.59]
X_2	Ground vertical settlement-2	mm	DB6–DB9	−17.18	2.18	[−21.32, −12.83]
X_3	Ground vertical settlement-3	mm	DB1, DB10–DB12	−3.94	1.98	[−8.89, 0.82]
X_4	Deflection of lateral wall-1	mm	P1–P4	27.87	12.90	[5.40, 53.80]
X_5	Deflection of lateral wall-2	mm	P5–P11	49.19	13.79	[10.60, 58.40]
X_6	Vertical displacement of wall	mm	Q1–Q10	15.13	3.93	[5.46, 21.07]
X_7	Settlement of electric power pipe-1	mm	DL1–DL5	−20.38	2.97	[−26.20, −14.20]
X_8	Settlement of electric power pipe-2	mm	DL6–DL10	7.66	2.50	[1.00, 12.30]
X_9	Settlement of rainwater pipe	mm	YS1–YS3	2.20	5.19	[−9.60, 9.20]

surement uncertainty. Herein, an equal number of data samples is randomly generated for each feature every day (sampling 6000 times). For illustration purposes, measured data of the feature X_1 on the first day (D_1–X_1) are also taken as an example to show the sampling results, as given in Fig. 11. Based on the best-fit distribution identified by MSE, the sampling data following the normal distribution can be quickly generated with a mean value of 3.81, a stan-

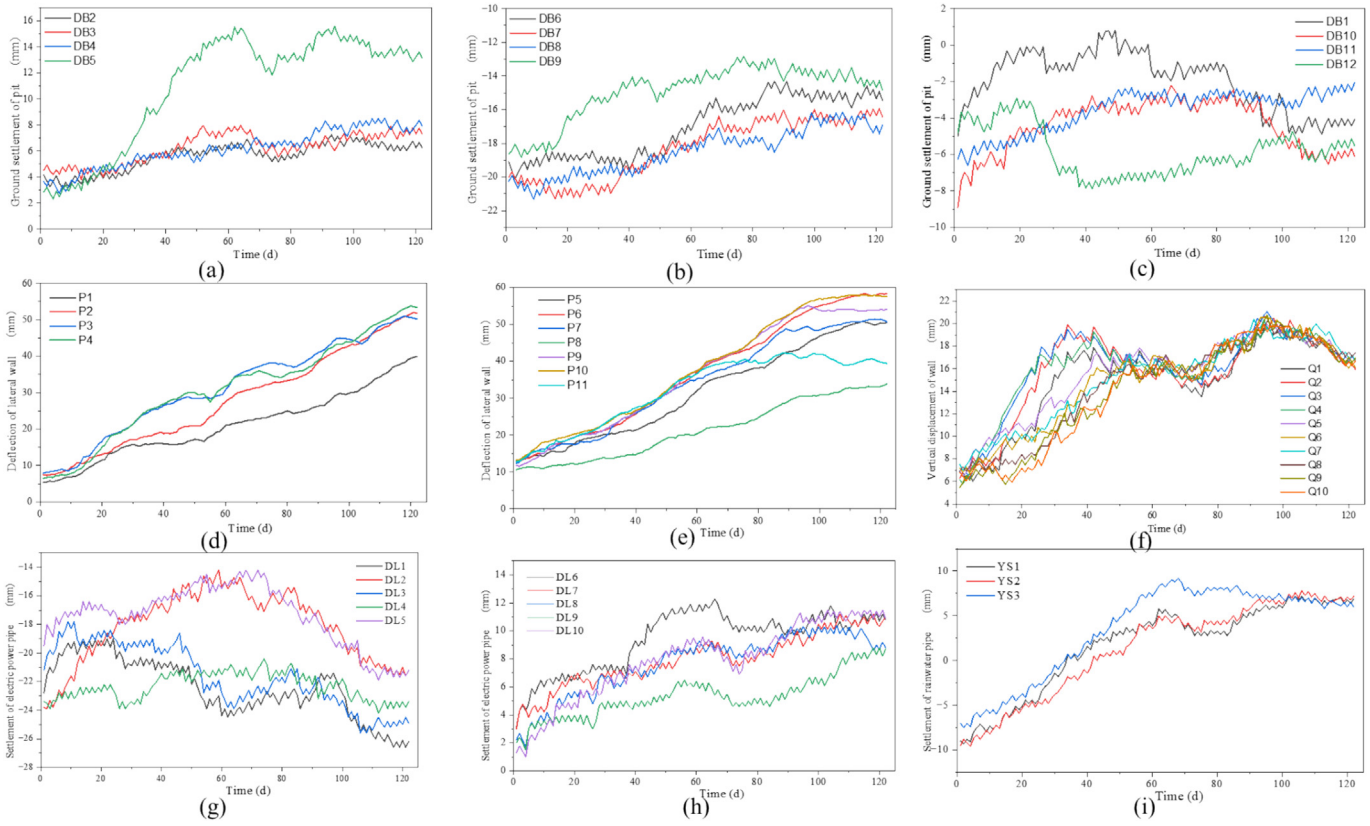

Fig. 7. Time-series measured data of nine selected features during the excavation process: (a) X_1, (b) X_2, (c) X_3, (d) X_4, (e) X_5, (f) X_6, (g) X_7, (h) X_8, and (i) X_9.

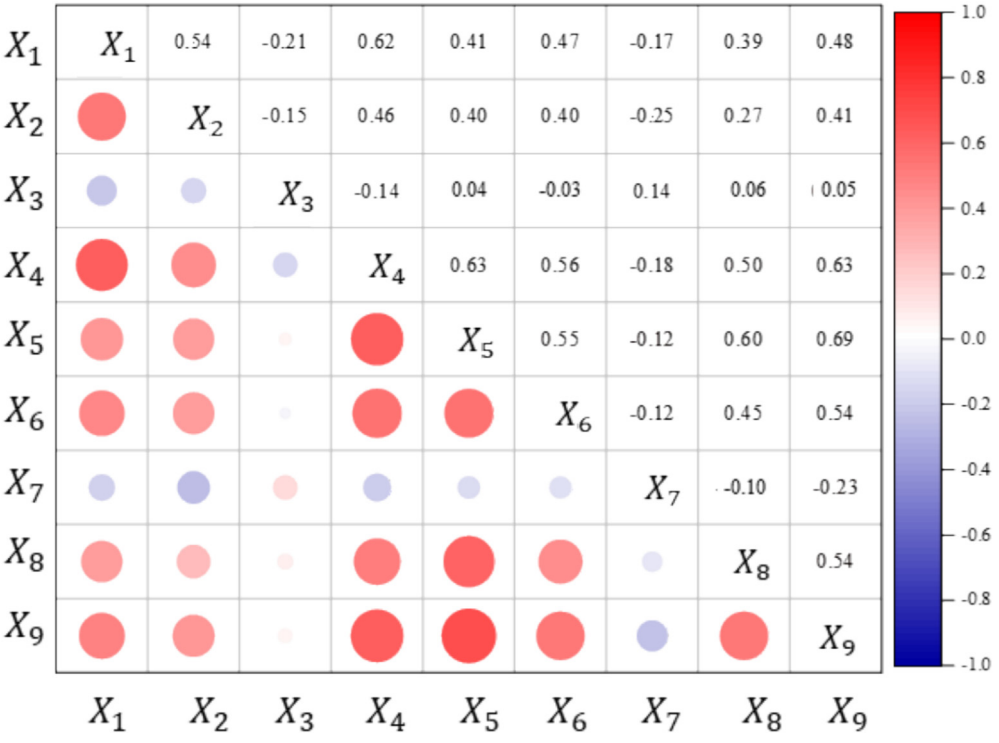

Fig. 8. Kendall coefficient matrix of the input features.

Table 2
MSE value for evaluating the fitting performance of the candidate distributions on measured data from the first monitoring day.

Feature	Candidate distribution			Best-fit distribution
	Normal	Lognormal	Weibull	
X_1	0.23	0.45	1.18	Normal
X_2	0.12	0.99	1.13	Normal
X_3	1.89	8.06	8.15	Normal
X_4	1.71	3.66	0.92	Weibull
X_5	2.96	1.53	1.50	Weibull
X_6	1.47	1.62	1.49	Normal
X_7	1.71	1.32	1.17	Weibull
X_8	0.66	0.49	0.81	Lognormal
X_9	1.82	1.90	2.23	Normal

Note: Each feature has one cell with color representing the smallest value of MSE and the corresponding distribution is considered as the best-fit distribution for the feature.

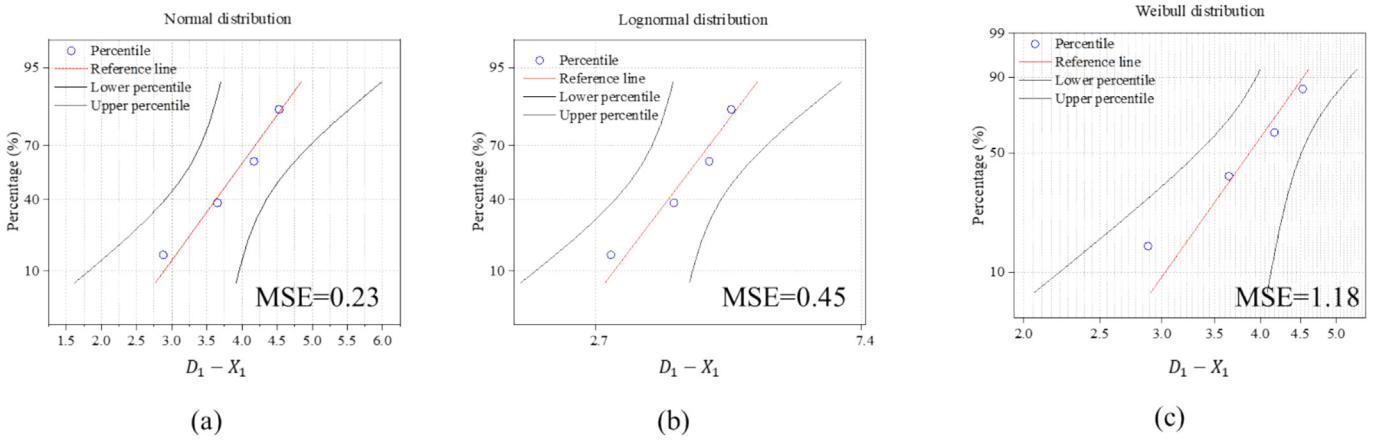

Fig. 9. Probabilistic modeling for the feature X_1 on the first day (D_1–X_1) using the three candidate distributions. (a) Normal distribution, (b) lognormal distribution, and (c) Weibull distribution.

dard deviation of 0.61, and a 95% confidence interval of mean in [3.79, 3.82]. The Monte Carlo simulation process is repeated for all the features collected each day, and the measurement uncertainty can be well captured. Subsequently, the sampling data points generated by Monte Carlo simulations are fed into the PM-LSTM model to make the excavation-induced risk prediction, allowing for capturing the risk status evolution of adjacent buildings under the careful consideration of uncertainty.

The sampled data is partitioned into 80% for training and 20% for testing, which are then used to input the PM-LSTM model for predicting daily risks to adjacent buildings based on excavation-induced ground settlement. Designed as a multi-layer neural network for function approximation, the PM-LSTM model is detailed in Table 3. The batch size is set as 32, a commonly used value balancing computational efficiency and gradient stability. While this setting is based on empirical results, further tuning via hyperparameter search (e.g., grid search, random search, Bayesian optimization) may enhance performance. Figure 12 illustrates the MSE loss function curve over 200 epochs, capturing both training and testing processes. Clearly, the MSE curve shows a converging trend, verifying the powerful learning ability of the established PM-LSTM model. The MSE value gradually decreases in the initial 10 epochs and then goes into stabilization as the PM-LSTM model continuously learns from the training data. After 200 iterations, the MSE reaches a value of around 0.005 for both training and testing, achieving precise predictions of ground settlement in the adjacent building. In addition,

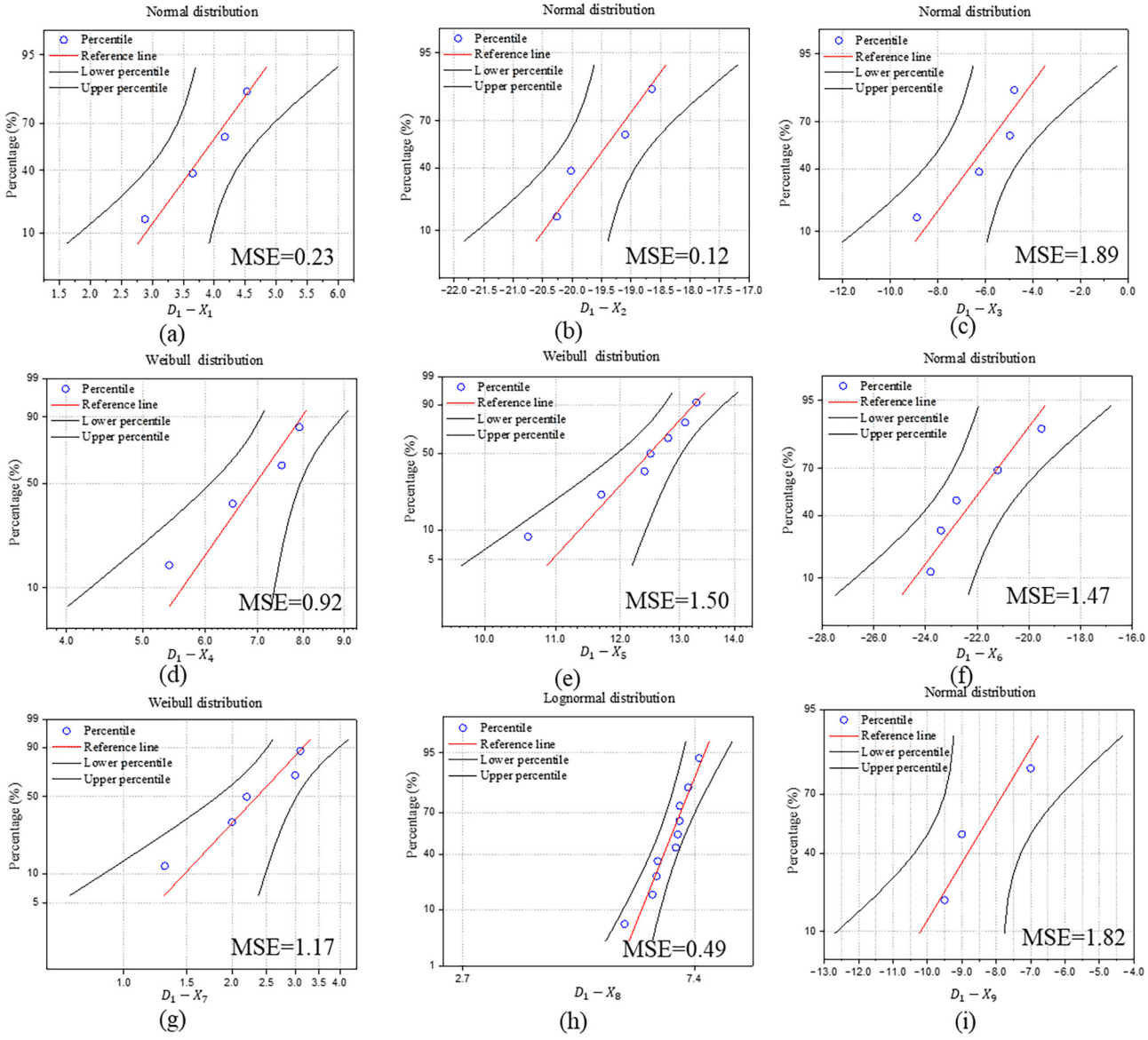

Fig. 10. Investigations for the best-fit distribution of the nine features (X_1–X_9) on the first day. (a) X_1, (b) X_2, (c) X_3, (d) X_4, (e) X_5, (f) X_6, (g) X_7, (h) X_8, and (i) X_9.

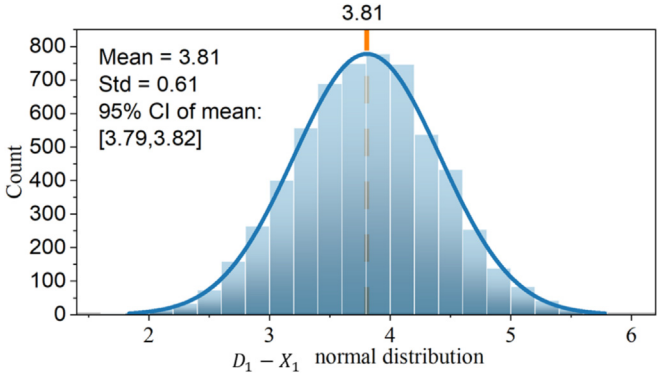

Fig. 11. Monte Carlo-based data sampling for the feature X_1 on the first day (D_1–X_1) under the best-fit distribution.

Table 3
Summary of the PM-LSTM model structure.

Layer	Type	Output shape	Parameter
1	LSTM	(32, 10, 128)	89 600
2	Dropout	(32, 10, 128)	0
3	LSTM	(32, 64)	49 408
4	Dropout	(32, 64)	0
5	Dense	(32, 8)	520

the MSE curves for the training set and test set exhibit similar convergence trends, indicating no occurrence of overfitting in predictions.

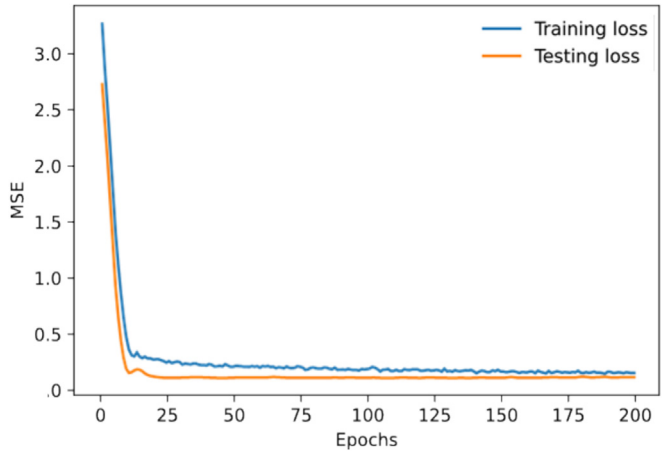

Fig. 12. MSE loss of the LSTM model training and testing for the ground settlement of the adjacent building caused by the foundation pit construction.

For evaluation purposes, Fig. 13(a) records the MSE values of the error between the real data and predicted data for each day, with an overall prediction error below 0.2. Figure 13(b) and (c) reveals that the proposed method could achieve an average MAE of 0.104 and 0.131 in the training and test set, respectively. These results indicate that the PM-LSTM model can predict excavation-induced risk, represented by the ground settlement of adjacent buildings, with high accuracy throughout the entire deep excavation process. Besides, while a longer monitoring period enhances the model's ability to capture more temporal patterns, the PM-LSTM framework remains sufficiently robust to handle shorter data periods without significant loss in performance. This flexibility is a notable advantage of the PM-LSTM model, as it can effectively accommodate varying data durations. Even with data durations shorter than 122 days, the model continues to perform reliably, with only minor variations in performance depending on the length of the data sequence.

3.4 Forward learning results

Under the appropriate network structure and hyperparameter combination, the PM-LSTM model in the forward learning process can supplement input samples under uncertainty modeling, and then dynamically predict the ground settlement of the adjacent building on behalf of excavation-induced risk. Noticeably, the high accuracy of the PM-LSTM-based predictions facilitates the estimation of the probability that the adjacent building will be at different risk levels at any given time. Additionally, the model allows for estimating the probability of transitioning to a new risk level for the first time each day. The detailed analysis is presented below.

(1) The PM-LSTM model can fully learn the simulated data, incorporating prior knowledge for temporal feature extraction, which can well capture the evolving trend of building ground settlement under the dynamic and uncertain excavation environment. By specifying prior distributions, PM-LSTM can produce informed predictions, especially in situations with limited data. It fits a small number of measured data for each response feature in the excavation system each day using certain probability distributions, resulting in sufficient samples via Monte Carlo simulations for PM-LSTM model training. This probabilistic framework incorporates information from the entire distribution of input data, enabling the estimation of adjacent building ground settlement as a range of possible outcomes with associated probabilities rather than a single deterministic value. This

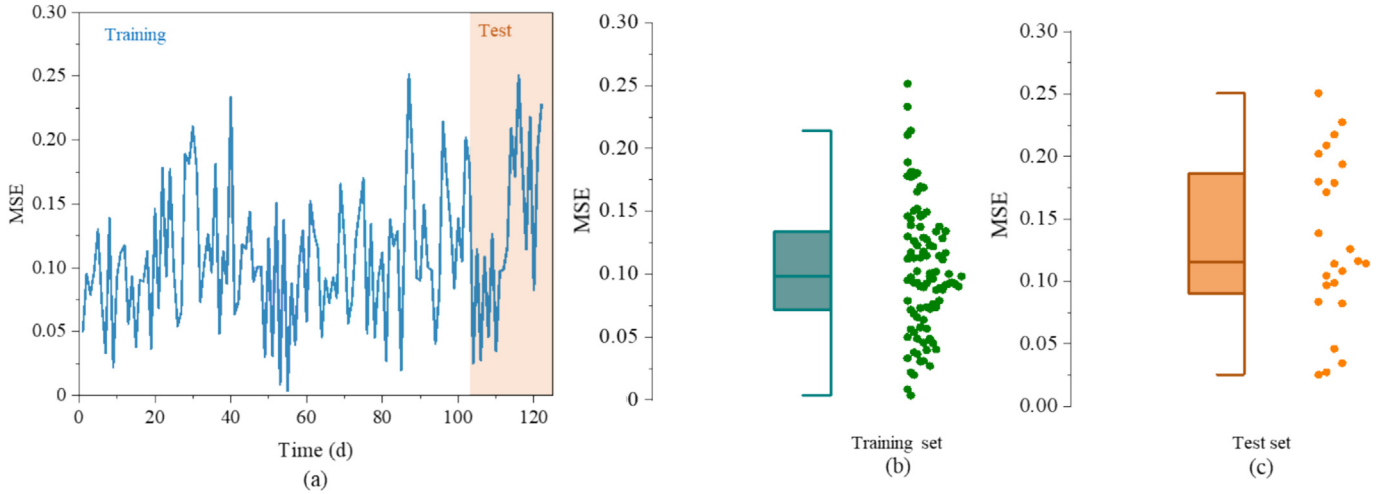

Fig. 13. Prediction performance evaluation of the PM-LSTM model. (a) MSE in the training and test set, (b) boxplot of MSE in the training set, and (c) boxplot of MSE in the test set.

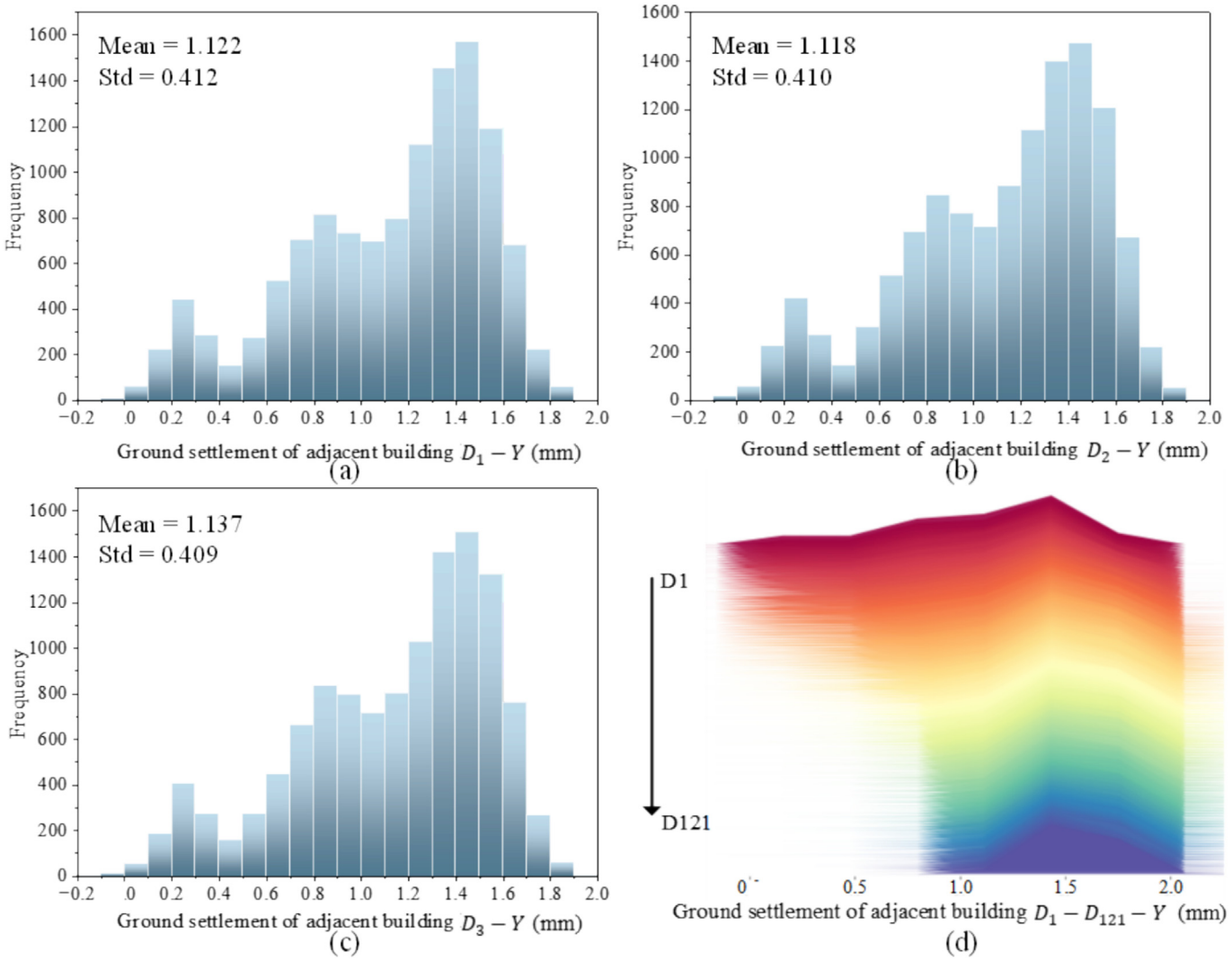

Fig. 14. Probabilistic prediction results about the ground settlement of the adjacent building using the established PM-LSTM: (a) the 1st day, (b) the 2nd day, (c) the 3rd day, and (d) the 1st day to the 121st day.

characteristic enhances the model's ability to make stable and reliable predictions amidst uncertainty. Figure 14(a)–(c) takes the probabilistic prediction results at the first three days as an example. Due to the higher frequency of occurrence, the adjacent building is likely to suffer from ground settlement caused by the excavation project in the range between 1.2 and 1.6 mm. As the excavation progresses, the PM-LSTM model continuously updates its predictions by learning from newly available data, thereby facilitating a dynamic process for generating probabilistic forecasts of ground settlement. The probability prediction results over 121 days are provided in Fig. 14(d), where each day has an estimated distribution to provide insights into the likelihood of the ground settlement occurring. Observably, the prediction values tend to become concentrated within a narrow range over time.

(2) Based on the prediction results regarding the ground settlement of the adjacent building, the risk status of the adjacent building can be evaluated to determine a specific risk level. The application of the PM-LSTM model extends beyond risk prediction to encompass risk assessment, thereby providing a comprehensive understanding of potential excavation-induced risks. Herein, the ground settlement threshold for the adjacent building is carefully set to quantitatively determine five risk levels donated as I, II, III, IV, and V, which is appropriate for the specific engineering situation as a single case study calculation. While the variations may appear small, the primary objective of this case study is to validate the effectiveness of our proposed PM-LSTM method. The identified risk levels and their corresponding control measures are summarized in Table 4. Generally, the higher settlement value or the excessive uplift deformation is

Table 4
Determination of five risk levels for the adjacent building.

Risk level	Description	Ground settlement range	Risk control measures
I	Safe	[1.4 mm, 1.5 mm]	To perform monitoring in a normal way
II	Low risk	[1.5 mm, 1.6 mm]	To perform monitoring in a normal way and to properly optimize the excavation process
III	Medium risk	[1.6 mm, 1.7 mm]	To increase the monitoring frequency for key objects, to increase the monitoring items, and to adjust the excavation process
IV	High risk	[1.7 mm, 1.8 mm]	To evaluate the excavation project, to take protective measures, and to adjust the excavation process
V	Extremely high risk	[1.8 mm, ∞]	To stop the excavation project, and to formulate a new excavation plan

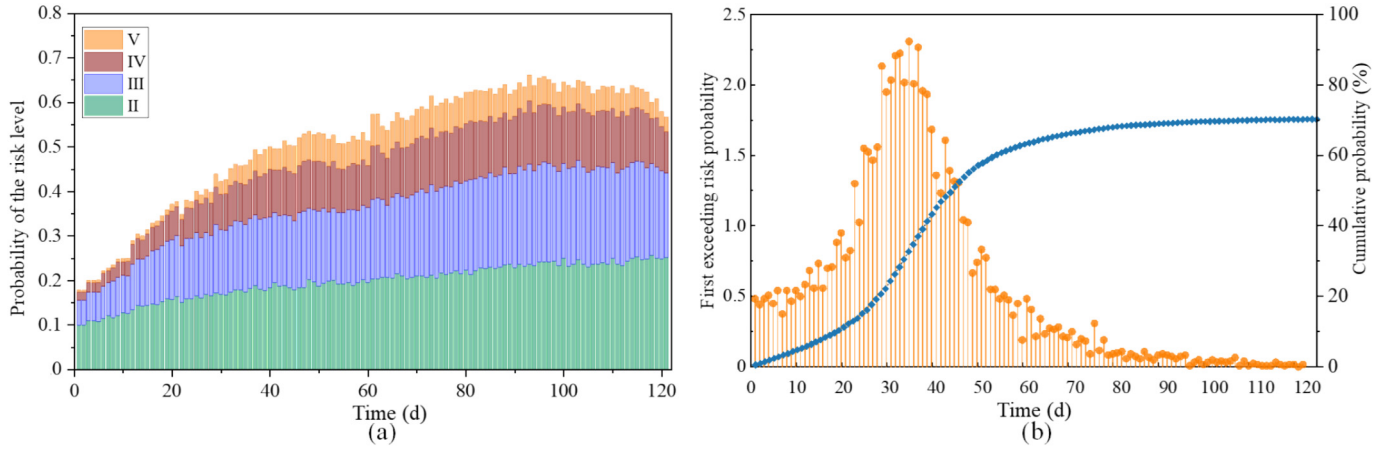

Fig. 15. Risk level evaluation for the adjacent building during the excavation procedure. (a) Probability of the adjacent building at the risk levels II–V, and (b) the first exceeding risk probability of excavation-induced settlement.

prone to pose more potential risks to the building safety. It is important to note that extreme threshold values, whether excessively small or large, may undermine robust risk management. However, the threshold values presented in the case study serve primarily as illustrative examples. These values do not affect the overall functionality or trustworthiness of the proposed framework. The core methodology remains valid regardless of the specific threshold values used, as the framework is designed to adapt to varying thresholds based on the context and the data available. According to Table 4 and Eqs. (16)–(20), the probability of the adjacent building falling into each of the five risk levels during the excavation process is depicted in Fig. 15(a), considering the dynamic and uncertain nature of the excavation system. Evidently, within the first 20 days, there is a rapid escalation in the probability of transitioning to higher risk levels, with a potential emergence of extremely high-risk (level V). After that, the probability of the adjacent building being in the high or extremely high-risk levels gradually increases and stabilizes towards the end. Overall, the adjacent building is more likely to be classified within the low or medium-risk levels (II or III), which aligns with the risk dynamics typically observed in real-world excavation scenarios.

(3) To enable timely risk alerts for the building, the first exceeding risk probability of the adjacent building is calculated using Eq. (20), under the assumption that no first-time failures have occurred in previous excavation days. It should be emphasized that this probability pertains to the building entering the extremely high-risk level (V) for the first time. Figure 15(b) presents the first exceeding risk probability of the building on each day of excavation. The first exceeding risk probability experiences a rapid increase at the beginning of the excavation project, which peaks at the value of 2.32% on the 36th day. This instability is attributed to complex soil conditions and inadequate structural support. Subsequently, as appropriate preventive or protective measures are implemented in response to actual excavation conditions, the construction site progressively stabilizes. Consequently, the first exceeding risk probability exhibits a declining trajectory, indicating a decreased likelihood of the adjacent building reaching

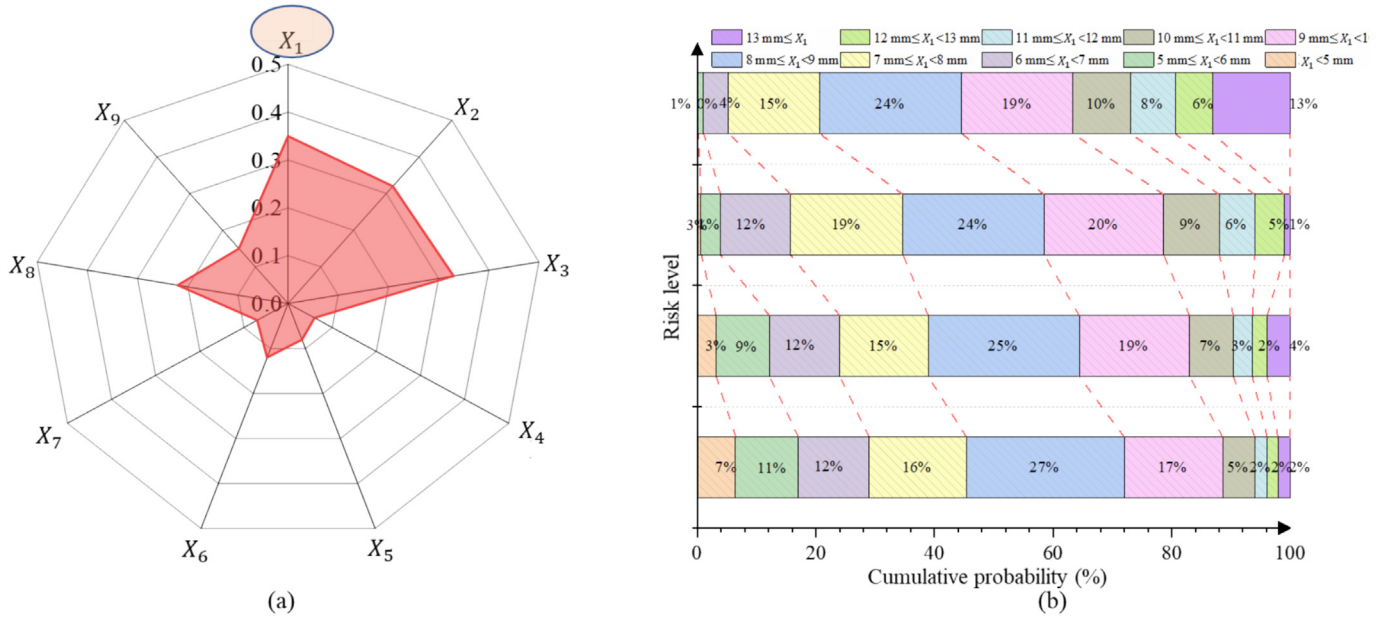

Fig. 16. Post-analysis results. (a) Sensitivity index for the nine response parameters, and (b) probability of response parameter X_1 in different intervals under different risk levels of the adjacent building.

the extremely high-risk level during the later stages of the excavation project. In particular, there is a high occurrence probability of shifting the building risk status to the risk level V during the excavation days of 29–39. Hence, special focus needs to be paid to this time period with relatively large values of the first exceeding risk probability, which can bring practical benefits of early warning and timely intervention to avoid the risk deterioration on the adjacent building. Another thing to be noted is that the cumulative probability for the first exceeding risk cannot reach 100%. This is likely due to the relatively high threshold set for risk classification, suggesting that the building may not encounter conditions that would push it into the extremely high-risk category.

3.5 Post-analysis results

To achieve a comprehensive understanding of the excavation-induced risks on adjacent buildings, the post-analysis techniques outlined above can be effectively applied to the developed PM-LSTM model. For one thing, sensitivity analysis can be employed to quantify the relative influence of key parameters on the risk status of adjacent buildings, identifying dominant factors driving potential hazards. For another, the PM-LSTM method can be carried out in a reverse learning process to infer the probability of specific response features falling within certain ranges, thereby triggering a high-risk level for the adjacent building. These post-analysis results can provide actionable insights for project managers, enabling the formulation of proactive risk mitigation strategies. The detailed analysis is presented below.

(1) Sensitivity analysis supports quantifying the contribution of each feature to the overall risk level of the adjacent building, thereby enabling resource allocation that prioritizes the control of these critical factors. When the risk level of the adjacent building reaches an extremely high level, the sensitivity index in Eq. (21) can be calculated to rank the relative importance of the influential features influencing the excavation-induced risk on the building. As visualized in Fig. 16(a), the feature sensitivity ranking is as follows: $X_1(0.35) > X_3(0.33) > X_2(0.32) > X_8(0.22) > X_9(0.15) > X_6(0.12) > X_5(0.08) > X_7(0.07) > X_4(0.06)$. Accordingly, the top three critical features are all related to the ground settlement of the foundation pit itself, aligning with common engineering practice that places significant emphasis on monitoring ground settlement during construction. To further reduce the high occurrence probability of risk events in the adjacent building, it is suggested to properly increase monitoring frequency for these top features X_1–X_3.

(2) Based on the implementation of PM-LSTM in an inverse direction, the cumulative probability for a pit response parameter falling within a specific interval can be obtained under conditions where the adjacent building is at a defined risk level. Given that feature X_1 has been identified as the most influential factor contributing to high risk in the adjacent building, the PM-LSTM model undergoes a reverse learning process to establish the non-linear relationship between the ground settlement of the building and that of the pit. Figure 16(b) takes X_1 as an example to show its cumulative probability across various

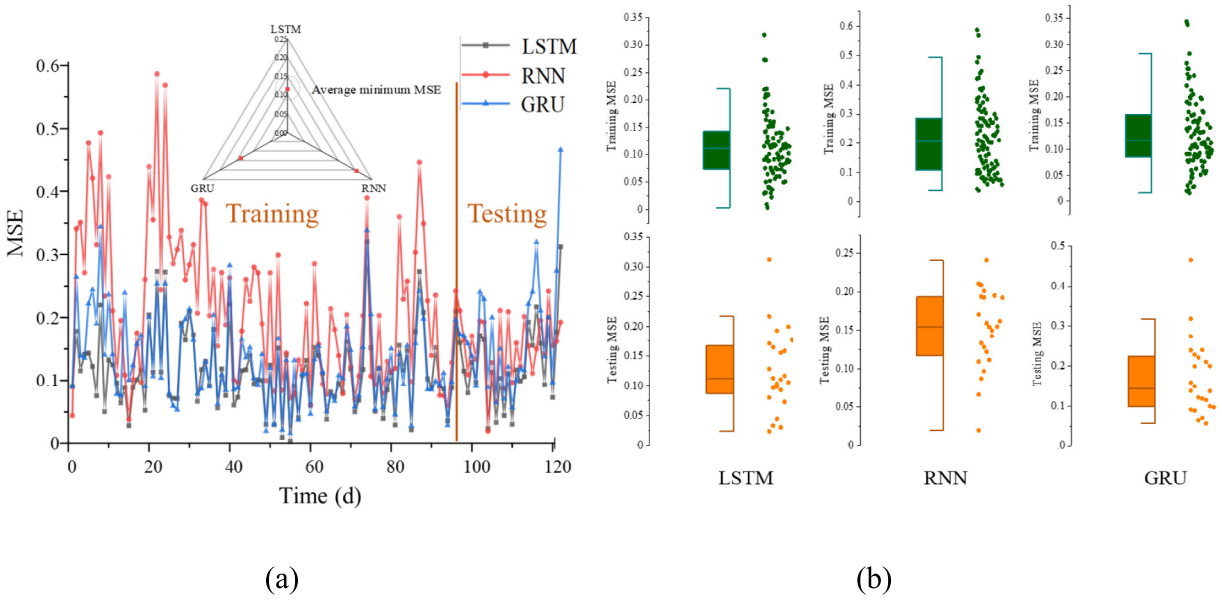

Fig. 17. Comparison of prediction performance of three deep learning models in exaction-induced risk prediction. (a) Time variant MSE of the three models, and (b) boxplots of MSE of the three models (top: training dataset, bottom: testing dataset).

value intervals when the adjacent building is at different risk levels. Observably, X_1 is prone to be in the range of [8 mm, 10 mm] with a probability larger than 43% regardless of the risk level. In particular, X_1 is more likely to cause the building to enter the high or extremely high-risk level when its value surpasses 10 mm. The cumulative probability of X_1 above 10 mm for driving the building into the risk level II to IV is measured at 11.4%, 17%, 19.6%, and 36.6%, respectively. Therefore, once the X_1 value goes beyond 10 mm, a risk warning can be issued, and managers can respond timely to potential risk events.

4 Discussion

In order to validate the superiority of the proposed Bayesian reasoning-based probabilistic deep learning method for excavation-induced risk prediction and early warning, a series of comparative experiments is performed using the same dataset. More specifically, the predictive accuracy of the proposed method is evaluated against two widely used time-series intelligent prediction models. Additionally, the robustness of the proposed method is tested by introducing white noise, which simulates uncertainties arising from external environmental factors and monitoring device inaccuracies. A detailed analysis of these evaluations is provided as follows:

(1) In the forward learning process, the proposed PM-LSTM model exhibits superior performance compared to two widely used time-series intelligent prediction models, namely RNN and GRU. To ensure a fair comparison of model prediction accuracy, the Bayesian hyperparameter optimization is conducted on these three deep learning models to effectively determine the optimal set of parameters. Also, MSE is used as the loss function, and Adam is taken as the optimizer. Figure 17 demonstrates the prediction performance evaluation based on MSE in both the training set and test set for the three deep learning models. It is evident that the MSE of LSTM, represented by the gray line, always maintains a low value throughout the excavation period, while the RNN model, indicated by the red line, displays less stability with larger error values and fluctuations in predicting daily building settlement. This suggests that the LSTM model, with its more complex network architecture and increased number of parameters, is better equipped to handle the intricacies of such prediction tasks. The average MSE of LSTM (0.109) indicates a clear improvement over the RNN (0.035 higher MSE) and GRU (0.101 higher MSE) models, highlighting the superior prediction performance of the PM-LSTM model.

(2) Uncertainties stemming from the surrounding environment and monitoring devices can compromise the accuracy of building risk perception, potentially leading to delayed responses. To address this, it is essential to incorporate these uncertainties into the calculation of the first exceeding risk probability for adjacent buildings, particularly with regard to the likelihood of reaching an extremely high-risk level (V). To assess the robustness of the PM-LSTM model against external interference, two levels of white noise—low and high—are introduced into the dataset. Low noise represents minor disturbances from data collection and environmental factors, while high

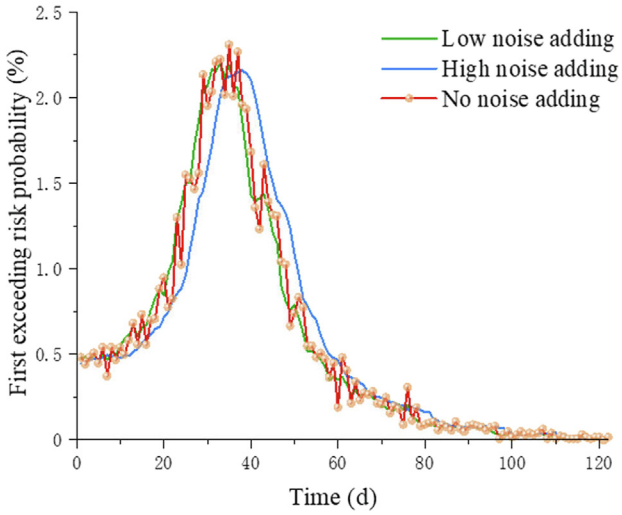

Fig. 18. Estimation of the first exceeding risk probability of the adjacent building to enter the extremely high-risk level (V) under different noise conditions.

noise represents more significant, abrupt variations. The augmented data is then used for excavation-induced risk prediction, determining the first exceeding risk probability for risk level V. Given the stochastic nature of noise addition, this process is repeated 1000 times, and the averaged probabilities are visualized in Fig. 18. Across all conditions, the highest probability of exceeding risk level V occurs between the 30th and 40th excavation day, confirming the PM-LSTM model's robustness. Specifically, the peak probabilities under low noise, no noise, and high noise conditions are 2.225% (33rd day), 2.308% (35th day), and 2.159% (38th day), respectively. The slight delay observed under high noise suggests that excessive interference may impact the model's ability to accurately capture risk evolution patterns.

5 Conclusions

This study proposes a data-driven and trustworthy approach for excavation-induced risk warning for adjacent buildings. The key innovation lies in the integration of Bayesian reasoning within a hybrid deep learning model that combines probabilistic modeling with the classical LSTM architecture. The resulting PM-LSTM model effectively handles uncertainties inherent in excavation projects while tracking the dynamic evolution of risk levels for nearby structures. Through a forward learning process, the PM-LSTM model estimates the probability of a building entering a specific risk state, enabling early risk detection and proactive alerts. The Bayesian framework further supports sensitivity analysis and reverse learning to identify key risk factors and inform mitigation strategies. Practically, the continuous integration of real-time project data into the PM-LSTM model provides robust and evidence-based support for developing reliable risk management strategies, thereby ensuring timely interventions and safe excavation progress.

The proposed Bayesian reasoning-based probabilistic deep learning method is validated in a real excavation project at Zone A of Jing'an Temple Station of Shanghai Metro. The key research findings are presented as follows: (1) Through forward learning, PM-LSTM can deliver a promising prediction performance on the evolution of risk states represented by the ground settlement of the adjacent building in a probabilistic manner. It is observed that the probability of buildings being risk-free gradually decreases as the excavation process advances. (2) Through reverse learning, the response parameter called ground settlement of the foundation pit can be quantitatively determined as the main checkpoint in the excavation process, since it, with a higher sensitivity index value, contributes more to the risk event on the adjacent building. Besides, once a specific risk level is assigned to the adjacent buildings, the posterior probabilities of all response parameters can be computed, offering valuable new insights for informed risk management. (3) Comparative experiments affirm the superior prediction accuracy of the proposed method over conventional RNN and GRU models, even under the influence of white noise. Furthermore, the model demonstrates notable robustness and can seamlessly transition to other adjacent buildings and infrastructures proximate to the targeted foundation pit, underscoring its potential for widespread application and generalization.

Data availability

The data used in this research are available on GitHub: https://github.com/pqcoop/UndSpacePaperData.git.

CRediT authorship contribution statement

Yue Pan: Writing – review & editing, Writing – original draft, Supervision, Project administration, Methodology, Funding acquisition, Formal analysis, Conceptualization. **Xuyang Li:** Writing – review & editing, Writing – original draft, Validation, Methodology, Investigation, Formal analysis. **Jianjun Qin:** Writing – review & editing, Writing – original draft, Supervision, Methodology, Investigation, Formal analysis, Conceptualization. **Jinjian Chen:** Writing – review & editing, Writing – original draft, Supervision, Methodology, Funding acquisition, Conceptualization. **Paolo Gardoni:** Writing – review & editing, Writing – original draft, Methodology, Conceptualization.

Declaration of competing interest

The authors declare that they have no known competing financial interests or personal relationships that could have appeared to influence the work reported in this paper.

Acknowledgement

This work was substantially supported by the National Natural Science Foundation of China (Grant No. 72201171) and the Shanghai Sailing Program (No. 22YF1419100).

References

Fu, Y., Chen, L., Xiong, H., Chen, X., Lu, A., Zeng, Y., & Wang, B. (2024). Data-driven real-time prediction for attitude and position of super-large diameter shield using a hybrid deep learning approach. *Underground Space, 15*, 275–297.

Hochreiter, S., & Schmidhuber, J. (1997). Long short-term memory. *Neural Computation, 9*(8), 1735–1780.

Jin, Y., Biscontin, G., & Gardoni, P. (2021). Adaptive prediction of wall movement during excavation using Bayesian inference. *Computers and Geotechnics, 137*, 104249.

Lin, S.-S., Shen, S.-L., Zhang, N., & Zhou, A. (2022). An extended TODIM-based model for evaluating risks of excavation system. *Acta Geotechnica, 17*(4), 1053–1069.

Ministry of Housing and Urban-Rural Development of the People's Republic of China (2019). *GB 50497—2019: Technical standard for monitoring of building excavation engineering*. China Planning Press (in Chinese).

Pan, Y., He, W., & Chen, J.-J. (2025). Spatiotemporal deep learning for multi-attribute prediction of excavation-induced risk. *Automation in Construction, 171*, 105964.

Pan, Y., & Qin, J. (2022). A novel probabilistic modeling framework for wind speed with highlight of extremes under data discrepancy and uncertainty. *Applied Energy, 326*, 119938.

Pan, Y., Qin, J., Hou, Y., & Chen, J.-J. (2024). Two-stage support vector machine-enabled deep excavation settlement prediction considering class imbalance and multi-source uncertainties. *Reliability Engineering & System Safety, 241*, 109578.

Pan, Y., Qin, J., Zhang, L., Pan, W., & Chen, J.-J. (2024). A probabilistic deep reinforcement learning approach for optimal monitoring of a building adjacent to deep excavation. *Computer-Aided Civil and Infrastructure Engineering, 39*(5), 656–678.

Pan, Y., & Zhang, L. (2023). Integrating BIM and AI for smart construction management: Current status and future directions. *Archives of Computational Methods in Engineering, 30*(2), 1081–1110.

Phoon, K.-K., Pan, Q., & Tang, C. (2024). Editorial for machine learning and AI for underground metaverse. *Underground Space, 19*, 1–3.

Qin, J. (2018). Improved Probabilistic Modeling of Wind Speed in the Context of Structural Risk Assessment. *KSCE Journal of Civil Engineering, 22*(3), 896–902.

Shen, S.-L., Lin, S.-S., & Zhou, A. (2023). A cloud model-based approach for risk analysis of excavation system. *Reliability Engineering & System Safety, 231*, 108984.

Song, W., Lu, C., Lin, J., Fang, C., & Liu, S. (2023). A low-quality PMU data identification method with dynamic criteria based on spatial-temporal correlations and random matrices. *Applied Energy, 343*.

Wang, X., Pan, Y., & Chen, J.-J. (2025). Digital twin with uncertainty-informed deep learning for prompt quantitative risk assessment of deep excavation. *Computer-Aided Civil and Infrastructure Engineering, online*.

Xue, Y., Shi, P., Jia, F., & Huang, H. (2022). 3D reconstruction and automatic leakage defect quantification of metro tunnel based on SfM-Deep learning method. *Underground Space, 7*(3), 311–323.

You, H., & Tian, Y. (2023). Research on the influence of deep foundation pit excavation on pile foundations of nearby buildings. *Proceedings of SPIE, 12511*, 125110T.

Zeng, Y., Atangana Njock, P. G., Xiong, W., Zhang, X.-L., & Shen, S.-L. (2023). Risks analysis of large diameter slurry shield tunneling in urban area. *Underground Space, 13*, 281–300.

Zhang, W., Gu, X., Tang, L., Yin, Y., Liu, D., & Zhang, Y. (2022a). Application of machine learning, deep learning and optimization algorithms in geoengineering and geoscience: Comprehensive review and future challenge. *Gondwana Research, 109*, 1–17.

Zhang, W., Han, L., Gu, X., Wang, L., Chen, F., & Liu, H. (2022b). Tunneling and deep excavations in spatially variable soil and rock masses: A short review. *Underground Space, 7*(3), 380–407.

Zhou, X., Pan, Y., Qin, J., Chen, J.-J., & Gardoni, P. (2024). Spatio-temporal prediction of deep excavation-induced ground settlement: A hybrid graphical network approach considering causality. *Tunnelling and Underground Space Technology, 146*, 105605.